Loss of muscle stem cells in aged mice is replenished by muscle-secreted niche factor G-CSF

Hu Li[#], Qian Chen[#], Changyin Li, Ran Zhong, Yixia Zhao, Dahai Zhu*****

and Yong Zhang*****

The State Key Laboratory of Medical Molecular Biology, Institute of Basic Medical Sciences, Chinese Academy of Medical Sciences and School of Basic Medicine, Peking Union Medical College, 5 Dong Dan San Tiao, Beijing 100005, P R China.

RUNNING TITLE: **Metabolic niche maintains muscle stem cells**

To whom correspondence should be addressed: Yong Zhang and Dahai Zhu, The State Key Laboratory of Medical Molecular Biology, Institute of Basic Medical Sciences, Chinese Academy of Medical Sciences and School of Basic Medicine, Peking Union Medical College, 5 Dong Dan San Tiao, Beijing 100005, P R China.

Tel:+86-10-6915-6949; Fax:+86-10-6510-5083; E-mail:yongzhang@ibms.pumc.edu.cn; dhzhu@pumc.edu.cn

Lead contact: Dahai Zhu, dhzhu@pumc.edu.cn

Summary

Function and number of muscle stem cells (satellite cells, SCs) declines with muscle aging. Although SCs are heterogeneous and different subpopulations have been identified, it remains unknown if a specific subpopulation of muscle SCs selectively decreases during aging and whether muscle metabolism plays a niche role in regulating the selected decline. Here, using single cell RNA sequencing, we show Pax7^{Hi} and Pax7^{Lo} cells represent two distinct subpopulations. We further find Pax7^{Hi} cells are not only enriched in glycolytic fibers but reduced in aged muscle. Further, we identify granulocyte-colony stimulating factor (G-CSF) as a muscle-secreted niche factor required for regulating the dynamic heterogeneity of Pax7 SCs in mice by promoting their asymmetric division. Intriguingly, we found an unappreciated role for MyoD in regulating transcription of G-CSF (*Csf3*) gene in a metabolism-dependent manner in muscle. Together, our findings uncover a metabolic niche role of muscle metabolism in regulating Pax7 SC heterogeneity in mice.

Key words: Pax7 Satellite Cells, Heterogeneity, Metabolic Niche, G-CSF, Asymmetric Division, Aged Mice

Highlights

1) Single cell RNA-seq unveils Pax7^{Hi} and Pax7^{Lo} cells are two distinct subpopulations

2) Pax7^{Hi} SCs are enriched in glycolytic fibers and reduced in aging muscle

3) Metabolic niche factor G-CSF is required for regulating dynamic change of Pax7 SCs

4) G-CSF replenishes Pax7^{Hi} cells by stimulating asymmetric division of Pax7^{Mi} cells

Introduction

Reduced tissue regenerative potential is one of the general hallmarks in mammalian aging (Rando, 2006) and decline in the number and function of adult stem cells are major causes that contribute to the failure of regeneration in several adult tissues during aging (Conboy et al., 2003; Molofsky et al., 2006; Nishimura et al., 2005; Rossi et al., 2005). However, the molecular mechanisms underlying this age-dependent loss of adult stem cells in tissue regeneration are largely unknown. In adult skeletal muscle, muscle stem cells, also known as satellite cells (SCs), reside in a quiescent state between the basal lamina and the muscle fiber sarcolemma. SCs are responsible for postnatal muscle growth and regeneration after injury. SCs are also heterogeneous where different subpopulations have unique features of self-renewal, proliferation, and differentiation during regeneration (Kuang et al., 2007; Rocheteau et al., 2012; Wilson et al., 2008). Pax7, a transcriptional factor, plays critical roles in regulating SC functions during development and regeneration (Sambasivan et al., 2011; Seale et al., 2000; von Maltzahn et al., 2013). It has been recently reported that Pax7-positive SCs (Pax7 SCs) are heterogeneous including $Pax7^{Hi}$ and $Pax7^{Lo}$ subpopulations (Rocheteau et al., 2012). However, little is known regarding the functional establishment and maintenance of the heterogeneity of Pax7 SCs during development. During aging, the decline in number and function of Pax7 SCs is attributable to the loss of skeletal muscle mass and strength as well as the decreased regenerative capacity of skeletal muscle. More intriguingly, it remains unclear if a specific subpopulation of Pax7 SCs decreases during aging and what are the dynamics of this heterogeneity in aged mice.

The microenvironment, or niche contributes significantly to the behaviors of adult stem cells, as first reported for germ stem cell niche of the *Drosophila* ovary (Xie and Spradling, 2000) and the hematopoietic stem cell niche in mammal (Schofield, 1978). However, little is known about which niche components are required to regulate the heterogeneity of adult stem cells. The identification of niche factors will help elucidate the molecular mechanisms underlying the establishment and maintenance of adult stem cell heterogeneity during development and physiological aging. In skeletal muscle, muscle stem cells were directly attached with two major types of muscle fiber which are defined based on their metabolic

capacity: slow-twitch oxidative fibers and fast-twitch glycolytic fibers (Schiaffino and Reggiani, 2011). Interestingly, there is a link between SC numbers/function and fiber metabolism, more SC cells on slow-twitch oxidative fibers than that on fast-twitch glycolytic fibers (Collins et al., 2005; Feldman and Stockdale, 1991; Lagord et al., 1998). Further, decline of SC numbers and function are correlated with fiber type switch from glycolytic fast-twitch to oxidative slow-twitch fiber during aging. These observations imply a possible effect of fiber metabolism on SC function and behavior during aging.

Skeletal muscle is a major secretory organ, and muscle fibers express and secrete various factors (e.g., IL-6 and FGF-2) that regulate skeletal muscle growth and regeneration in autocrine, paracrine, or endocrine manners (Pedersen and Febbraio, 2008, 2012). Given that muscle fibers exhibit metabolic heterogeneity, secrete factors that have paracrine function, and exhibit intimate contact with Pax7 SCs, we hypothesized that muscle fibers function as a metabolic niche for skeletal muscle SCs by supplying requisite factors that in turn regulate the heterogeneity of Pax7 SCs during development and aging in mice. In the present study, we tested this hypothesis using several experimental approaches. First, using single cell RNA sequencing, we demonstrate that $Pax7^{Hi}$ and $Pax7^{Lo}$ cells are two distinct subpopulations of satellite cells. More significantly, we uncover that the number of $Pax7^{Hi}$ subpopulation satellite cells is significantly reduced in aged mice. Mechanistically, we reveal that altered heterogeneity of Pax7 SCs is regulated by myofiber-secreted granulocyte colony-stimulating factor (G-CSF), which is metabolically regulated by MyoD in myofibers and in turn interacts with its receptor, G-CSFR, on Pax7 SCs. This interaction is required for establishing and maintaining the $Pax7^{Hi}$ SC subpopulation in adult and physiological aged mice by promoting the asymmetric division of $Pax7^{Hi}$ and $Pax7^{Mi}$ SCs.

Results

Characterization of $Pax7^{Hi}$ and $Pax7^{Lo}$ SCs by single-cell RNA sequencing

Quiescent $Pax7^{Hi}$ and $Pax7^{Lo}$ cells were isolated by FACS based on levels of GFP (Pax7) from tibialis anterior muscle of *Pax7-nGFP* mice (Figure S1A-S1C) and subjected to single cell RNA sequencing (scRNA-Seq). We profiled 1,243 $Pax7^{Hi}$ cells and 3,960 $Pax7^{Lo}$ cells. The typical number of detectable genes ranged approximately from 1000 to 2000 genes in individual

cells. Unsupervised hierarchal clustering analysis with the single-cell RNA transcriptome indicated that quiescent Pax7^{Hi} and Pax7^{Lo} cells belong to two distinctly clustered subpopulations (Figure 1A， Figure S1D). Transcriptome comparisons between Pax7^{Hi} and Pax7^{Lo} subpopulations identified 428 differentially expression genes (P<0.05, LogFC>0.25), which exhibit distinct gene signatures (Figure 1B). Furthermore, GO-enriched analysis of the differentially expressed genes between those two subpopulations consistently validated the previously described features (Figure S1E-S1G): genes related to stemness were highly expressed in the Pax7^{Hi} subpopulation and genes related to myogenic differentiation were highly expressed in the Pax7^{Lo} subpopulation (Figure 1C). Additionally, we found that Pax7^{Hi} cells expressed high levels of mitochondrial genes (Figure 1D; Figure S1H), suggesting that Pax7^{Hi} cells are adapted to oxidative metabolism. Finally, several molecular markers for either Pax7^{Hi} or Pax7^{Lo} cells were identified in this study. *Ptprb*, *Pvalb*, *Acta1*, *Hbb-bt* are for Pax7^{Hi} cells and *Cdh15*, *Rcan2*, *Rps28*, *Acta2* for Pax7^{Lo} cells (Figure 1E and 1F). The expression patterns of these genes were validated by real-time PCR (Figure S1I). Together, the high resolution analysis using single-cell RNA sequencing provides evidence that Pax7^{Hi} and Pax7^{Lo} cells represent two distinct subpopulations in mice. Therefore, the Pax7^{Hi} and Pax7^{Lo} cells used in the following experiments were FACS-sorted based on the levels of Pax7 expression as previously reported (Rocheteau et al., 2012; Wu et al., 2015).

Pax7^{Hi} cells are significantly reduced in aged mice

Given that the number and functionality of Pax7 SCs decline with age and Pax7^{Hi} cells with more stem-like properties represent a reversible dormant stem cell state and generate distinct daughter cell fates by asymmetrically segregating template DNA during muscle regeneration. We assessed whether the percentage of Pax7^{Hi} cells was altered in aged mice. Satellite cells were sorted from TA muscle of young and aged mice, respectively. FACS profiling revealed that the percentage of Pax7^{Hi} SCs was severely reduced in the TA muscle fibers of aged mice compared to young mice (Figure 2A-2C). Consistent with this, we observed low levels of *Pax7* and stemness-related genes *CD34*, but high levels of myogenic differentiation-related genes

(*MyoD* and *MyoG*) in Pax7 SCs freshly isolated from aged TA muscle fibers versus young TA muscle fibers (Figure 2D). We also examined expression of newly identified genes as markers for either $Pax7^{Hi}$ or $Pax7^{Lo}$ cells, respectively. We found lower levels of $Pax7^{Hi}$ marker genes expression (*mt-Nd1*, *mt-Co2* and *mt-Co3*) but higher levels of $Pax7^{Lo}$ marker genes expression (*Rcan2*, *Cdh15*) in Pax7 SCs freshly isolated from aged TA muscle fibers versus young TA muscle fibers (Figure 2E). Consistently, we observed that the activation of Pax7 SCs was significantly accelerated in the cells freshly isolated from aged TA muscle fibers versus the young TA muscle fibers (Figure 2F and 2G). Taken together, these results from aged mice demonstrate that $Pax7^{Hi}$ cells were significant reduced in aged mice.

Glycolytic metabolism of myofiber is required for the maintenance of $Pax7^{Hi}$ SC

To identify niche components in skeletal muscle that might be required for the maintenance of $Pax7^{Hi}$ cells in aged mice, we analyzed the transcriptomes of aged TA muscle and young TA muscle by RNA sequencing. RNA-seq results from aged TA muscle and young TA muscle identified a large number of differentially regulated genes (Figure 2H). Gene ontology (GO) analyses of biological processes highlighted the changes in a number of genes encoding metabolic regulators were observed in the transition from young to aged muscle (Figure 2I and 2J). The expression of genes corresponding to proteins that regulate lipid metabolic processes was upregulated (Figure 2I; Figure S2A), whereas that of genes regulating glucose metabolic processes was downregulated in aged TA muscle (Figure 2J; Figure S2B and S2C). To further confirm the metabolic shift during aging, we performed histochemical staining for α-glycerophosphate dehydrogenase (α-GPDH) and succinate dehydrogenase (SDH), which are enriched in glycolytic and oxidative myofibers, respectively. Aged TA muscle had higher SDH and lower α-GPDH enzymatic activities compared to young TA muscles (Figure S2D). Altogether, these results indicate that muscle metabolism was shifted from a glycolytic to oxidative state during aging as previously reported (Holloszy et al., 1991).

Since skeletal muscle composed of glycolytic myofiber and oxidative myofiber and SCs were directly attached with muscle fibers, we reasoned that metabolism of muscle fibers as a

metabolic niche regulating the heterogeneity of Pax7 SC cells. To this end, we examined the distributions of the Pax7^{Hi} subpopulations in tibialis anterior (TA, predominantly glycolytic) and soleus (Sol, mainly oxidative) muscle fibers from the same individual *Pax7-nGFP* reporter mice. Interestingly, the percentage of Pax7^{Hi} SCs sorted from glycolytic TA muscle fibers was significantly higher than that sorted from oxidative Sol muscle fibers of the same animal (Figure 3A-3C), indicating that the Pax7^{Hi} SC subpopulation was enriched in glycolytic muscle fibers of these mice. Consistent with this, we observed higher levels of *Pax7* and stemness-related genes (*CXCR4* and *CD34*) but lower levels of myogenic differentiation-related genes (*MyoG*) in Pax7 SCs freshly isolated from TA muscle fibers versus Sol muscle fibers of the same mice (Figure 3D). We also examined expression of newly identified genes as markers for either Pax7^{Hi} or Pax7^{Lo} cells, respectively. We found higher levels of Pax7^{Hi} marker genes expression (*mt-Nd1*, *mt-Co2*, *mt-Co3*, *Ptprb* and *Hbb-bt*) but lower levels of Pax7^{Lo} marker genes expression (*Rcan2* and *Cdh15*) in Pax7 SCs freshly isolated from TA muscle fibers versus Sol muscle fibers of the same animal (Figure 3E). Consistently, we observed that the activation of Pax7 SCs was significantly delayed in the cells freshly isolated from TA muscle fibers versus the corresponding Sol muscle fibers (Figure 3F and 3G). To rule out the possibility that enrichment of Pax7^{Hi} SCs in glycolytic TA muscle fibers is mediated by fiber type per se, we examined correlation between fiber type/fiber metabolism and the heterogeneity of Pax7 SC cells in TA and Sol muscle at 3 and 10 weeks, respectively. We found that the fiber type had been remarkably different between TA and Sol muscle of 3 weeks mice (Figure S3A-S3B), but the significant difference in muscle metabolism was occurred till 10 weeks (Figure S3C-S3E). Interestingly, the significant difference in the percentage of Pax7^{Hi} cells between TA and Sol muscle was only observed at 10 weeks but not at 3 weeks (Figure 3H), indicating that metabolic features of myofibers rather than muscle contraction associate with establishment of Pax7^{Hi} subpopulations in TA muscle. Our results show for the first time that Pax7 SCs are remarkably heterogeneous between glycolytic and oxidative muscle fibers. This heterogeneity may be related to the metabolic activity of these muscle fibers under normal physiological conditions.

To further confirm the causal effects of fiber metabolism on Pax7 SC heterogeneity in mice, we examined the distribution of the Pax7^{Hi} SC subpopulation in the TA muscle of the well-characterized *PPARβ* transgenic (TG) mice, which exhibits significantly enriched oxidative muscle fibers and dramatically decreased glycolytic muscle fibers (Gan et al., 2013) (Figure S3F-S3H). Consistent with the remarkably reduced glycolytic metabolism seen in *PPARβ* TG mice, the percentage of Pax7^{Hi} SCs was significantly reduced in the TA muscle fibers of *PPARβ* TG mice compared to those of wild-type (WT) littermates (Figure 3I-3K). In agreement with this finding, the mRNA levels of *Pax7*, *CXCR4* and *CD34* were also lower, but the levels of *MyoD* and *MyoG* were higher, in Pax7 SCs freshly isolated from the TA muscle of *PPARβ* TG mice compared to those of WT mice (Figure S3I). Moreover, the activation of Pax7 SCs freshly isolated from the TA muscle fibers of *PPARβ* TG mice was significantly faster than that observed in WT littermates (Figure S3J and S3K). Together, these results support the notion that glycolytic metabolism favors the establishment and maintenance of Pax7^{Hi} cells in mice.

Muscle-released G-CSF is a metabolic niche factor required for establishment and maintenance of Pax7^{Hi} SCs in mice

Based on the above observations, we hypothesized that cytokines highly expressed and secreted by glycolytic muscle fibers might function as niche factors required to maintain Pax7^{Hi} SC subpopulation in aged mice. To identify the muscle-secreted factors responsible for the loss of satellite cell during aging, we analyzed the global gene expression changes occurring within TA muscle during physiological aging. We found that muscle-secreted granulocyte colony-stimulating factor (G-CSF) was particularly interesting because it was significant downregulated in aged TA muscle than young TA muscle (Figure 4A). Also, G-CSF was more highly expressed and secreted by glycolytic versus oxidative muscle fibers in adult mice (Figure 4B and 4C), and it was remarkably reduced in the TA muscle fibers of *PPARβ* TG versus WT adult mice (Figure 4D). Therefore, we reasoned that G-CSF might be a Pax7 SC niche factor required for the established enrichment of Pax7^{Hi} SCs in glycolytic TA muscle in adult mice. To test this possibility, we freshly isolated Pax7 SCs from total muscle tissues of *Pax7-nGFP* mice,

and treated the cells with either G-CSF or PBS (control) for 48 hr. G-CSF treatment significantly increased the percentage of Pax7^{Hi} SCs compared to the PBS control (Figure 4E and 4F), indicating that G-CSF plays a functional role in modulating Pax7^{Hi} SCs *in vitro*. This was further supported by significant upregulation of Pax7 in SCs treated with G-CSF for 48 hr (Figure S4A). To further confirm that G-CSF is a niche factor required for Pax7^{Hi} SCs establishment, we generated *Pax7-nGFP;Csf3r*$^{-/-}$ mice by crossing *Csf3r*$^{-/-}$ mice with *Pax7-nGFP* reporter mice. When Pax7 SCs isolated from the *Pax7-nGFP;Csf3r*$^{-/-}$ mice were treated with either G-CSF or PBS for 48 hr, G-CSF failed to increase the percentage of Pax7^{Hi} SCs from *Pax7-nGFP;Csf3r*$^{-/-}$ mice (Figure 4E and 4F). Consistent with these *in vitro* findings, when we compared the distribution of Pax7^{Hi} SCs in glycolytic TA of WT mice and *Pax7-nGFP;Csf3r*$^{-/-}$ mice, the percentage of Pax7^{Hi} SCs was significant reduced in those of *Pax7-nGFP;Csf3r*$^{-/-}$ mice (Figure 4G and 4H). We next examined the mRNA levels of *Csf3* and marker genes for the muscle fiber type (*Myh 4*) and muscle fiber metabolism (*HK2* and *PFK1*) in the TA muscles of *Pax7-nGFP;Csf3r*$^{-/-}$ and *Pax7-nGFP* WT mice. Our results ruled out the possibility that the observed effects in the *Pax7-nGFP;Csf3r*$^{-/-}$ mice were due to a reduction in *Csf3* expression or an alteration of muscle fiber metabolism (Figure S4B and S4C). Moreover, we did not find any difference in the *Csf3* mRNA levels of immune cells sorted from the TA or Sol muscle fibers of *Pax7-nGFP;Csf3r*$^{-/-}$ mice (Figure S4D and S4E). Collectively, these findings demonstrate that muscle-released G-CSF and its receptor on Pax7 SCs are required to establish the Pax7^{Hi} SC subpopulation in mice.

Expression of *Csf3* gene encoding G-CSF is metabolically regulated by MyoD in muscle cells

We then asked if G-CSF is indeed a metabolic niche factor secreted by muscle fibers, then the *Csf3* gene encoding G-CSF should be metabolically regulated in muscle cells. To test this, we examined *Csf3* gene expression in C2C12 myotubes with enhanced glycolytic activity by culturing them in pyruvate-free medium (Chen et al., 2016) (Figure S5A and S5B). The expression of *Csf3* gene was significantly increased in myotubes that exhibited higher

glycolytic activity (Figure 5A), indicating that the transcription of *Csf3* gene was indeed regulated by the enhancement of glycolytic metabolism in myotubes. To determine how expression of *Csf3* gene is metabolically controlled by glycolytic activity of myofiber, we analyzed the 2-kb upstream of the transcriptional start site of the *Csf3* promoter and six E-boxes were found in this region (Figure S5C), suggesting that metabolically-mediated expression of *Csf3* gene might be regulated by myogenic regulatory factors such as MyoD in muscle cells. Therefore, we examined MyoD expression in myotubes cultured with pyruvate-free medium and found that enhanced glycolytic activity in the myotubes cultured with pyruvate-free medium also significantly elevated MyoD expression (Figure 5A). In addition, we also observed that similar to *Csf3*, *MyoD* was also more prominently expressed in glycolytic TA muscle fibers compared to oxidative Sol muscle fibers in mice (Figure S5D and S5E). To determine if MyoD metabolically regulates *Csf3* expression *in vivo*, expression of *Csf3* was assessed in TA muscles of MyoD-knockout (MyoD-KO) mice and WT mice. Consistently, levels of *Csf3* mRNA were significantly reduced in the glycolytic TA muscles of MyoD-knockout (MyoD-KO) mice compared to WT mice (Figure 5B), indicating that MyoD is a transcriptional factor for regulating *Csf3* expression in muscle cells. To further confirm this possibility, we overexpressed MyoD in C2C12 muscle cells and found that MyoD overexpression remarkably augmented *Csf3* transcription (Figure S5F). MyoD-mediated transcription of *Csf3* gene was further corroborated by using a luciferase reporter system driven by the E-box-containing 2-kb region upstream of the *Csf3* promoter. Luciferase reporter activity was assayed in both C3H-10T1/2 fibroblasts and C2C12 cells transiently transfected with MyoD in the presence of the reporter construct. Forced expression of MyoD in either fibroblasts or C2C12 cells significantly activated the luciferase reporter gene driven by the 2-kb *Csf3* promoter, compared with the negative control (Figure 5C; Figure S5G). In addition, we examined luciferase reporter gene activity in the TA muscles of MyoD-KO and WT mice. Consistent with the results of our *in vitro* assays, the TA muscles of MyoD-KO mice showed significantly less luciferase activity than those of WT mice (Figure 5D). Together, our *in vitro*

and *in vivo* analyses reveal that MyoD regulates the *Csf3* gene transcription in muscle cells.

Next we examined whether the glycolytically-mediated transcription of the *Csf3* gene is regulated by MyoD in muscle cells. First, we checked *Csf3* expression in both *MyoD*-knockdown (MyoD-KD) and control C2C12 myotubes with enhanced glycolytic activity. The metabolic reprogramming-induced upregulation of *Csf3* expression seen in control myotubes was completely abolished in the MyoD-KD myotubes (Figure S5H and S5I), indicating that MyoD is required for the metabolically induced expression of *Csf3* in myotubes. To further confirm this observation, we assessed luciferase reporter gene activity driven by the *Csf3* promoter in MyoD-KD and control C2C12 myotubes cultured in the presence or absence of pyruvate. Indeed, significantly increased reporter gene activity was found to be induced by glycolytic metabolism only in control myotubes, but not in MyoD-KD myotubes (Figure 5E). Interestingly, enhanced glycolytic activity did not alter the expression of the endogenous *MyoG* gene (Figure S5J) or the activity of a luciferase reporter gene driven by the *MyoG* proximal promoter (Figure S5K), revealing that metabolically-mediated *Csf3* transcription is specifically regulated by MyoD in the muscle cells. Finally, functional analysis of *Csf3* gene promoter for identifying the E-boxes in its promoter required for MyoD-controlled metabolic transcription was performed by reporter gene assays with various truncated mutants of the *Csf3* gene promoter. Reporter assay showed that truncation of *Csf3* promoter containing the E-box (-1519bp, -1791bp, -1853bp) response to glycolytic metabolism, suggesting that the E-boxes (-1519bp, -1791bp, -1853bp) are required for MyoD-mediated *Csf3* transcription (Figure 5F, Figure S5C). To further corroborate the observation, we performed MyoD ChIP-seq on differentiated myotubes cultured in the presence or absence of pyruvate. Significantly, we found that enhanced glycolytic metabolism enriched MyoD binding on *Csf3* promoter but not in *MyoG* promoter (Figure 5G). This was further confirmed by MyoD ChIP-PCR on *Csf3* promoter and MyoG promoter (Figure 5H; Figure S5L and S5M). Taken together, our results not only provide molecular evidence to confirm that G-CSF is a muscle fiber secreted niche factor but also most interestingly uncover an unexpected metabolic role for MyoD as a

transcriptional factor in regulating *Csf3* gene expression in mature muscle.

Muscle-derived G-CSF promotes the asymmetric division of Pax7 SCs

Next, we explored the molecular mechanism through which muscle-derived and MyoD-regulated G-CSF acts as a Pax7 SC niche factor to modulate the heterogeneity of Pax7 SCs. We first assessed the expression of *Pax7* in SCs following G-CSF treatment. Interestingly, at 24 hr post-treatment, there was no obvious change in *Pax7* mRNA expression in Pax7 SCs sorted from *Pax7-nGFP* mice (Figure S6A), but these levels were significantly enhanced at 48 hr post-treatment (Figure S4A). These results suggest that the G-CSF-mediated enrichment of the $Pax7^{Hi}$ SC subpopulation most likely occurs through cell division of Pax7 SCs, rather than through an increase of *Pax7* expression in these cells.

As the self-renewal of SCs was proposed to be regulated by asymmetric division (Kuang et al., 2007; Troy et al., 2012) and G-CSFR was recently reported to be asymmetrically distributed in about 20% activated Pax7 SCs (Hayashiji et al., 2015), we hypothesized that G-CSF might mediate the heterogeneity of Pax7 SCs by promoting their asymmetric division via its interaction with the asymmetrically distributed G-CSFR on the Pax7 SCs. To test this possibility, we first performed time-lapse imaging of cell division in cultured Pax7 SCs sorted from *Pax7-nGFP* mice (Figure 6A-6C; Movie1) and in single fibers isolated from the extensor digitorum longus (EDL) muscles of *Pax7-nGFP* mice (Figure S6B-S6D; Movie 2). As expected, SCs underwent asymmetric division, each giving rise to one $Pax7^{Hi}$ cell and one $Pax7^{Lo}$ cell (Figure 6A-6C; Figure S6B-S6D). Next, we used several approaches to experimentally test our notion that G-CSF regulated the percentage of the $Pax7^{Hi}$ SC subpopulation by promoting their asymmetric division. Firstly, we assayed co-segregation of template DNA strands in the Pax7 cells. The TA muscles of 10-week-old *Pax7-nGFP* mice were injured by intramuscular injection of CTX. EdU labeling was used to monitor the co-segregation of template DNA (72 hr post injury), and BrdU was added to ensure that cells continued to divide during this period (8 hr post EdU) (Figure 6D). We ensured that all of the cells were EdU positive cells by performing immunostaining of EdU at T1 (Figure S6E). To determine whether Pax7 cell displayed

asymmetric division in response to G-CSF, we sorted Pax7 SCs and treated them with G-CSF in growth medium for 12 hr to complete cell division. In this paradigm, template DNA-retaining and -excluding cells would be EdU-positive or -negative, respectively (Figure 6E). We found that 12.5% of cells generated from Pax7 SCs were EdU-negative, suggesting that a subpopulation of Pax7 SCs underwent co-segregation of template DNA (Figure 6F). Notably, the EdU-negative daughter cells were primarily $Pax7^{Lo}$ SCs (Figure 6E). Significantly, G-CSF treatment increased the percentage of template DNA co-segregation in Pax7 SCs (Figure 6F), suggesting that G-CSF maintained $Pax7^{Hi}$ SCs by promoting the asymmetric divisions. To further confirm these observations, we determined probability of template DNA co-segregation in Pax7 SCs from *Csf3r*$^{-/-}$ mice, and found that significant reduced percentage of template DNA co-segregation in Pax7 SCs from *Csf3r*$^{-/-}$ mice (Figure 6G).

As G-CSFR was recently reported to be asymmetrically distributed in about 20% of activated Pax7 SCs (Hayashiji et al., 2015), we reasoned that the asymmetric distribution of G-CSFR response to G-CSF mediated asymmetric division. Firstly, single fibers isolated from the EDL muscles of *Pax7-nGFP* mice were treated with G-CSF for 48 hr and immunostained with anti-G-CSFR (Figure 6H). Notably, G-CSF treatment significantly increased the percentage of asymmetrically dividing Pax7 SCs, as characterized by the asymmetric distributions of G-CSFR (Figure 6I). To further substantiate this observation, we calculated the percentage of $EdU^{+/-}$ doublets with asymmetric distribution of G-CSFR. Indeed, the $EdU^{+/-}$ doublets exhibited a lower percentage of G-$CSFR^{+/+}$ cells with symmetrically distributed G-CSFR, and a significantly higher percentage of G-$CSFR^{-/+}$ cells with asymmetric distribution of G-CSFR (Figure 6J and 6K). The frequency of asymmetric G-CSFR distribution was consistent with the co-segregation of template DNA. Together, these results demonstrate that G-CSF promotes the asymmetric division of Pax7 SCs.

The G-CSF replenishes $Pax7^{Hi}$ cells by stimulating asymmetric division of $Pax7^{Mi}$ cells

Since reduced $Pax7^{Hi}$ cells in aged mice is correlated with fiber metabolism shift from glycolytic to oxidative, we then test whether enhanced glycolytic fiber metabolism could

rejuvenate Pax7^{Hi} cells in aged mice. As endurance exercise can significantly increase the glycolytic activity of muscle fibers (Heath et al., 1983), we examined percentage of Pax7^{Hi} SCs in TA muscles of aged mice in which glycolytic muscle metabolism was enhanced by endurance exercise. As expected, exercise significantly augmented the glycolytic activity in the TA muscles of aged mice compared to those of sedentary aged mice (Figure S7A). Notably, FACS analysis revealed that the percentage of Pax7^{Hi} SC subpopulation was dramatically increased in the TA muscles of exercised aged mice compared to sedentary aged mice (Figure 7A and 7B). Most significantly, we found that the percentage of Pax7^{Hi} SCs in the TA muscles of exercised aged mice was replenished almost to the level seen in untrained young mice (Figure 7A and 7B). These results indicate that enhanced glycolytic metabolism of myofiber rejuvenate Pax7^{Hi} cells in aged mice.

Given that exercise replenished Pax7^{Hi} cells through enhanced glycolytic metabolism of myofiber in aged mice (Figure 7A and 7B) and more interestingly, we also found that expression of *Csf3* is significantly reduced in TA muscles of aged mice and exercise significantly restored *Csf3* expression in the same fibers of aged mice (Figure S7B). Based on those observations, it is conceivable that exercise-induced G-CSF might functionally restore Pax7^{Hi} cells in TA muscles of aged mice. To test this, we subjected *Pax7-nGFP;Csf3r*$^{-/-}$ and *Pax7-nGFP* WT mice to endurance exercise. Indeed, exercise significantly augmented the *Csf3* RNA levels of TA muscles from both exercised *Pax7-nGFP* WT and *Pax7-nGFP;Csf3r*$^{-/-}$ mice compared to those of sedentary *Pax7-nGFP* WT and *Pax7-nGFP;Csf3r*$^{-/-}$ mice (Figure S7C). However, the percentage of Pax7^{Hi} SCs was only increased in the TA muscles of exercised *Pax7-nGFP* WT mice, but not in those of exercised *Pax7-nGFP;Csf3r*$^{-/-}$ mice (Figure 7C -7E). Collectively, our results reveal that muscle-derived G-CSF acts as a metabolic niche factor required for maintaining the Pax7^{Hi} SC subpopulation in physiologically aged mice. These results indicate that enhanced glycolytic metabolism of myofiber rejuvenate Pax7^{Hi} cells in aged SCs by regulating *Csf3* expression.

Next, we asked from which subpopulations Pax7 SCs (Pax7^{Lo}, Pax7^{Mi} and Pax7^{Hi}) contribute

to the replenishment of $Pax7^{Hi}$ SCs in aged mice after exercise. For this purpose, we further sorted $Pax7^{Mi}$ from *Pax7-nGFP* mice, and performed single cell RNA-seq. We profiled 5212 $Pax7^{Mi}$ cells and the detectable genes ranged approximately from 1000 to 2000 genes in individual cells. Then we combined the data of $Pax7^{Hi}$ and $Pax7^{Lo}$ (Figure 1A) with the data of $Pax7^{Mi}$ and visualized the cells in two dimensions according to their expression profiles by t-SNE projections. Our result showed that $Pax7^{Mi}$ cells are more closed to $Pax7^{Hi}$ cells (Figure 7F). Heatmaps of SCs profiles revealed normalized expression of the top variable genes in each subtype, and the expression pattern of $Pax7^{Mi}$ cells were similar with $Pax7^{Hi}$ cells (Figure 7G). Also, the markers of $Pax7^{Hi}$ cells in $Pax7^{Mi}$ cells were higher than $Pax7^{Lo}$ cells (Figure S7D and S7E). Hence, we reasoned that both $Pax7^{Hi}$ and $Pax7^{Mi}$ cells response to G-CSF to undergo asymmetric division. Consistently, we found that $Pax7^{Mi}$ SCs had more cells with asymmetric distribution of G-CSFR, followed by the $Pax7^{Hi}$ subpopulation, and then the $Pax7^{Lo}$ cell subpopulation, which had a very low percentage (Figure 7H and 7I). To further determine which cell subpopulation(s) displayed asymmetric division in response to G-CSF, we used FACS to sort $Pax7^{Hi}$, $Pax7^{Mi}$, and $Pax7^{Lo}$ SCs and treated them with G-CSF, respectively. We found that 36% of cells generated from $Pax7^{Hi}$ SCs and 10% of those generated from $Pax7^{Mi}$ SCs were EdU-negative, suggesting that most $Pax7^{Hi}$ SCs and some $Pax7^{Mi}$ SCs underwent co-segregation of template DNA (Figure 7J). G-CSF treatment increased the percentage of template DNA co-segregation in both $Pax7^{Hi}$ and $Pax7^{Mi}$ SCs (Figure 7J), suggesting that G-CSF enriched $Pax7^{Hi}$ SCs by promoting the asymmetric divisions of both $Pax7^{Hi}$ and $Pax7^{Mi}$ SCs. To further confirm these observations, we used flow cytometry to analyze template DNA co-segregation. After the cells finished their first cell division *in vitro*, ~56% of the $Pax7^{Hi}$ daughter cells were $EdU^{+}/BrdU^{+}$ and ~44% were $EdU^{-}/BrdU^{+}$, whereas ~18% of the $Pax7^{Mi}$ generated cells were $EdU^{-}/BrdU^{+}$ (Figure S7F). We also found that G-CSF treatment increased the percentage of template DNA co-segregation in both $Pax7^{Hi}$ and $Pax7^{Mi}$ SCs (Figure S7F). Together, these results suggest that G-CSF significantly enriches the percentage of $Pax7^{Hi}$ SCs by promoting the co-segregation of template DNA in both $Pax7^{Hi}$ and $Pax7^{Mi}$ SCs. As $Pax7^{Hi}$ SCs generate

distinct daughter cell fates by asymmetrically segregating template DNA strands to the stem cell (Rocheteau et al., 2012), only the Pax7^{Hi} cells themselves are not sufficient to enrich Pax7^{Hi} cells. The remarkable number of Pax7^{Mi} SCs with asymmetric distribution of G-CSFR provides a molecular basis for the G-CSF-mediated enrichment of Pax7^{Hi} SCs, which are generated through the asymmetric division of Pax7 SCs from the Pax7^{Mi} SC subpopulation.

Finally, we examined the signaling pathway(s) involved in the G-CSF-mediated enrichment and maintenance of Pax7^{Hi} SCs. As G-CSF is known to activate the Stat3 signaling pathway in Pax7 SCs (Hara et al., 2011), we tested whether G-CSF regulated Pax7^{Hi} subpopulation through this pathway. As reported, G-CSF activated Stat3 pathway and upregulated the downstream target genes in Pax7 SCs, but the Stat3 inhibitor significantly blocked effects of G-CSF (Figure S7G and S7H). FACS-sorted Pax7^{Hi}, Pax7^{Mi}, and Pax7^{Lo} SCs were further treated with G-CSF in the presence or absence of the Stat3 inhibitor 5,15 DPP. G-CSF enriched the Pax7^{Hi} cell subpopulations in both Pax7^{Hi} and Pax7^{Mi} cell cultures, as indicated above, but treatment with the Stat3 inhibitor significantly abolished this enrichment (Figure 7K). These data indicate that G-CSF enriches Pax7^{Hi} cells through the G-CSF-GCSFR-Stat3 axis. Collectively, our results offer multiple lines of experimental evidence showing that the G-CSF/G-CSFR/Stat3 axis is indispensably required to the establish Pax7^{Hi} SC subpopulation in mice, and that it acts by promoting the asymmetric division of Pax7 SCs.

Discussion

Cell metabolism has been shown to intrinsically and cell-autonomously regulate cellular functions in various types of cells, especially in cancer cells (Carey et al., 2015; Moussaieff et al., 2015; Ryall et al., 2015). However, it was not previously known whether tissue metabolism plays an extrinsic and non-cell-autonomous role in modulating cell functions *in vivo*. A recent *in vitro* study reported that stem cell functions are modulated by the metabolic interplay between supporting Paneth cells and intestinal Lgr5^{+} crypt base columnar cell (Lgr5+CBCs)(Rodriguez-Colman et al., 2017; Roper and Yilmaz, 2017). Here, we used various mouse genetic models to show for the first time that muscle fiber metabolism plays an *in situ* metabolic niche role in establishing and maintaining Pax7 SC heterogeneity in adult and

physiologically aged mice. Thus, we reveal that the local metabolic activity of a tissue can provide *in situ* niche signaling to regulate stem cell functions *in vivo*. To our knowledge, our findings provide the first evidence that a tissue metabolism per se can act as a metabolic niche in regulating behaviors of stem cells during development and aging in a living organism.

Skeletal muscle is the most abundant endocrine organ and exerts its functional roles by secreting various factors (Pedersen and Febbraio, 2008, 2012). Muscle SCs are located between the sarcolemma and the basal lamina of the muscle fibers which provide an immediate niche for the SCs by secreting different kinds of factors (Chakkalakal et al., 2012). However, only a few of the niche factors have been identified. For example FGF2 was an aged muscle fiber-released cytokine that acts locally as an extrinsic factor to regulate muscle stem cell quiescence in aged mice (Chakkalakal et al., 2012). Actually, the muscle SCs are directly associated with two types of metabolically different fibers: glycolytic fibers and oxidative fibers. This locally metabolic environment of muscle fibers with different metabolic activity has been considered as a metabolic stem cell niche; however, this metabolic niche hypothesis has not been investigated experimentally. Using this unique metabolic system, we herein report on identification and molecular characterization of the metabolic niche factor G-CSF. We show that the G-CSF is highly secreted from glycolytic muscle fibers and its expression is metabolically regulated by MyoD in muscle fibers. Functionally, the muscle fiber-secreted G-CSF is required for establishing and maintaining the $Pax7^{Hi}$ SC subpopulation in adult and physiological aged mice. Mechanistically, the muscle fiber-released G-CSF promotes the asymmetric division of $Pax7^{Hi}$ and $Pax7^{Mi}$ SCs by interacting with its receptor, G-CSFR, on Pax7 SCs in mice. To our knowledge, this is the first identified metabolic niche factor which is functionally required for regulating stem cell heterogeneity. The significance of our findings in general is that we provide molecular mechanism to conceptually prove metabolic niche hypothesis.

An unexpected finding of this study is the transcriptional activity of MyoD in mature muscle in mice. MyoD has long been regarded only as a master transcription factor with critical roles in controlling myogenic lineage specification during embryonic skeletal muscle development and activation of Pax7 SCs in response to muscle injury in adult mice (Cornelison et al., 2000; Megeney et al., 1996). Herein, we intriguingly found that MyoD predominately expressed in

glycolytic muscle and metabolically regulated transcription of muscle-secreted G-CSF gene *Csf3* in mature muscle. Mechanistically, we show that enhanced glycolytic metabolism of myotube significantly enriched MyoD binding on *Csf3* promoter but not on the promoter of myogenic differentiation gene *MyoG*. These results for the first time reveal that MyoD is a multifunctional transcription factor involved in regulating expression of either myogenic genes or metabolic-regulated genes in mature muscle. A major question for future studies is how the specificity of MyoD transcriptional activity is achieved in different biological contexts. Better understanding of this question will be greatly facilitated by identification of MyoD-interacting cofactors in various biological settings. Taken together, these findings provide a framework to investigate the unanticipated and novel role of MyoD and examine the broad function of this cell-lineage specific transcription factor.

Heterogeneity is one hallmark of adult stem cells. However, it remains unclear how this heterogeneity is established and maintained during development and aging. In this report, using single cell RNA seq, we are the first to demonstrate that $Pax7^{Hi}$ and $Pax7^{Lo}$ muscle stem cells sorted based on the levels of Pax7 expression represent two distinct bona fide subpopulations in mice and $Pax7^{Mi}$ cells were more similar to $Pax7^{Hi}$ cells. Most strikingly, our approaches in this study allow us to reveal the dramatically decreased percentage of $Pax7^{Hi}$ SCs in the glycolytic muscle fibers of physiologically aged mice (from 10% in adult mice to 2.7% in aged mice). Aging causes a deterioration of muscle function and regeneration that most likely reflects a decline in stem cell number and function. $Pax7^{Hi}$ SCs are characterized as quiescent SCs with a high regenerative capacity, so the age-related reduction of $Pax7^{Hi}$ SCs could account for the decline in muscle regeneration and repair in the aged mice. More remarkably, the reduction of the $Pax7^{Hi}$ SC subpopulation in the muscle fibers of aged mice can be rescued by the exercise-induced up-regulation of G-CSF. A recent study showed that G-CSFR is asymmetrically distributed in about 20% of activated Pax7 SCs (Hayashiji et al., 2015). Interestingly, we found that the percentage of Pax7 SCs with asymmetrically distributed G-CSFR differed significantly among the three Pax7 SC subpopulations; it was highest in $Pax7^{Mi}$, followed by $Pax7^{Hi}$, and then $Pax7^{Lo}$. In addition, we also found that $Pax7^{Mi}$ cells is very similar to $Pax7^{Hi}$ cells based on the gene expression signatures from single cell RNA sequencing. It therefore seems logical to propose a model in which $Pax7^{Mi}$ SCs might represent an intermediate population of

transitionally amplified Pax7 SCs that function as a reserve of Pax7 SCs from which active SCs are replenished, protecting the muscle stem cells from becoming exhausted under homeostasis and particularly following injury or during aging. Taken together our findings not only decipher a molecular mechanism that contributes to maintaining quiescent Pax7^{Hi} SCs in aged mice, but also suggest a subpopulation-based targeting strategy for treating age-related muscle loss (e.g., sarcopenia) or muscular dystrophy.

Acknowledgments

We greatly thank Yunning Geng and Huimin Liao from Bio-reach Co., Ltd., for their technical support of our time-pulse imaging experiments, and Dr. Zhenji Gan for providing the *PPARβ* transgenic mice. This work was supported by grants from the National Basic Research Program of China (2016YFA0100703, 2015CB943103), the National Natural Science Foundation of China (91540206, 31471289, 31471377), and the CAMS Initiative for Innovative Medicine (2016-I2M-1-017).

Author contributions

DZ conceived the project, coordinated the study, and wrote the paper. HL designed and performed the experiments. QC performed single cell RNA library construction and ChIP DNA library construction. CL performed the screening of muscle-secreted factors. RZ and YXZ performed the luciferase reporter gene assays. YZ helped draft the figure legends and experimental procedures of the manuscript. All authors approved the final version of the manuscript.

References

Carey, B.W., Finley, L.W., Cross, J.R., Allis, C.D., and Thompson, C.B. (2015). Intracellular alpha-ketoglutarate maintains the pluripotency of embryonic stem cells. Nature *518*, 413-416.

Chakkalakal, J.V., Jones, K.M., Basson, M.A., and Brack, A.S. (2012). The aged niche disrupts muscle stem cell quiescence. Nature *490*, 355-360.

Chen, W.W., Freinkman, E., Wang, T., Birsoy, K., and Sabatini, D.M. (2016). Absolute Quantification of Matrix Metabolites Reveals the Dynamics of Mitochondrial Metabolism. Cell *166*, 1324-1337 e1311.

Collins, C.A., Olsen, I., Zammit, P.S., Heslop, L., Petrie, A., Partridge, T.A., and Morgan, J.E. (2005). Stem cell function, self-renewal, and behavioral heterogeneity of cells from the adult muscle satellite cell niche. Cell *122*, 289-301.

Conboy, I.M., Conboy, M.J., Smythe, G.M., and Rando, T.A. (2003). Notch-mediated restoration of regenerative potential to aged muscle. Science *302*, 1575-1577.

Cornelison, D.D., Olwin, B.B., Rudnicki, M.A., and Wold, B.J. (2000). MyoD(-/-) satellite cells in single-fiber culture are differentiation defective and MRF4 deficient. Dev Biol *224*, 122-137.

Feldman, J.L., and Stockdale, F.E. (1991). Skeletal muscle satellite cell diversity: satellite cells form fibers of different types in cell culture. Dev Biol *143*, 320-334.

Gan, Z., Rumsey, J., Hazen, B.C., Lai, L., Leone, T.C., Vega, R.B., Xie, H., Conley, K.E., Auwerx, J., Smith, S.R., *et al.* (2013). Nuclear receptor/microRNA circuitry links muscle fiber type to energy metabolism. The Journal of clinical investigation *123*, 2564-2575.

Hara, M., Yuasa, S., Shimoji, K., Onizuka, T., Hayashiji, N., Ohno, Y., Arai, T., Hattori, F., Kaneda, R., Kimura, K., *et al.* (2011). G-CSF influences mouse skeletal muscle development and regeneration by stimulating myoblast proliferation. The Journal of experimental medicine *208*, 715-727.

Hayashiji, N., Yuasa, S., Miyagoe-Suzuki, Y., Hara, M., Ito, N., Hashimoto, H., Kusumoto, D., Seki, T., Tohyama, S., Kodaira, M., *et al.* (2015). G-CSF supports long-term muscle regeneration in mouse models of muscular dystrophy. Nat Commun *6*, 6745.

Heath, G.W., Gavin, J.R., 3rd, Hinderliter, J.M., Hagberg, J.M., Bloomfield, S.A., and Holloszy, J.O. (1983). Effects of exercise and lack of exercise on glucose tolerance and insulin sensitivity. J Appl Physiol Respir Environ Exerc Physiol *55*, 512-517.

Holloszy, J.O., Chen, M., Cartee, G.D., and Young, J.C. (1991). Skeletal muscle atrophy in old rats: differential changes in the three fiber types. Mech Ageing Dev *60*, 199-213.

Kuang, S., Kuroda, K., Le Grand, F., and Rudnicki, M.A. (2007). Asymmetric self-renewal and commitment of satellite stem cells in muscle. Cell *129*, 999-1010.

Lagord, C., Soulet, L., Bonavaud, S., Bassaglia, Y., Rey, C., Barlovatz-Meimon, G., Gautron, J., and Martelly, I. (1998). Differential myogenicity of satellite cells isolated from extensor digitorum longus (EDL) and soleus rat muscles revealed in vitro. Cell Tissue Res *291*, 455-468.

Megeney, L.A., Kablar, B., Garrett, K., Anderson, J.E., and Rudnicki, M.A. (1996). MyoD is required for myogenic stem cell function in adult skeletal muscle. Genes Dev *10*, 1173-1183.

Molofsky, A.V., Slutsky, S.G., Joseph, N.M., He, S., Pardal, R., Krishnamurthy, J., Sharpless, N.E., and Morrison, S.J. (2006). Increasing p16INK4a expression decreases forebrain progenitors and neurogenesis during ageing. Nature *443*, 448-452.

Moussaieff, A., Rouleau, M., Kitsberg, D., Cohen, M., Levy, G., Barasch, D., Nemirovski, A., Shen-Orr, S., Laevsky, I., Amit, M., *et al.* (2015). Glycolysis-mediated changes in acetyl-CoA and histone acetylation control the early differentiation of embryonic stem cells. Cell Metab *21*, 392-402.

Nishimura, E.K., Granter, S.R., and Fisher, D.E. (2005). Mechanisms of hair graying: incomplete

melanocyte stem cell maintenance in the niche. Science *307*, 720-724.

Pedersen, B.K., and Febbraio, M.A. (2008). Muscle as an endocrine organ: focus on muscle-derived interleukin-6. Physiological reviews *88*, 1379-1406.

Pedersen, B.K., and Febbraio, M.A. (2012). Muscles, exercise and obesity: skeletal muscle as a secretory organ. Nature reviews Endocrinology *8*, 457-465.

Rando, T.A. (2006). Stem cells, ageing and the quest for immortality. Nature *441*, 1080-1086.

Rocheteau, P., Gayraud-Morel, B., Siegl-Cachedenier, I., Blasco, M.A., and Tajbakhsh, S. (2012). A subpopulation of adult skeletal muscle stem cells retains all template DNA strands after cell division. Cell *148*, 112-125.

Rodriguez-Colman, M.J., Schewe, M., Meerlo, M., Stigter, E., Gerrits, J., Pras-Raves, M., Sacchetti, A., Hornsveld, M., Oost, K.C., Snippert, H.J., *et al.* (2017). Interplay between metabolic identities in the intestinal crypt supports stem cell function. Nature *543*, 424-427.

Roper, J., and Yilmaz, O.H. (2017). Metabolic Teamwork in the Stem Cell Niche. Cell Metab *25*, 993-994.

Rossi, M.A., Mash, D.C., and deToledo-Morrell, L. (2005). Spatial memory in aged rats is related to PKCgamma-dependent G-protein coupling of the M1 receptor. Neurobiol Aging *26*, 53-68.

Ryall, J.G., Dell'Orso, S., Derfoul, A., Juan, A., Zare, H., Feng, X., Clermont, D., Koulnis, M., Gutierrez-Cruz, G., Fulco, M., *et al.* (2015). The NAD(+)-dependent SIRT1 deacetylase translates a metabolic switch into regulatory epigenetics in skeletal muscle stem cells. Cell Stem Cell *16*, 171-183.

Sambasivan, R., Yao, R., Kissenpfennig, A., Van Wittenberghe, L., Paldi, A., Gayraud-Morel, B., Guenou, H., Malissen, B., Tajbakhsh, S., and Galy, A. (2011). Pax7-expressing satellite cells are indispensable for adult skeletal muscle regeneration. Development *138*, 3647-3656.

Schiaffino, S., and Reggiani, C. (2011). Fiber types in mammalian skeletal muscles. Physiological reviews *91*, 1447-1531.

Schofield, R. (1978). The relationship between the spleen colony-forming cell and the haemopoietic stem cell. Blood cells *4*, 7-25.

Seale, P., Sabourin, L.A., Girgis-Gabardo, A., Mansouri, A., Gruss, P., and Rudnicki, M.A. (2000). Pax7 is required for the specification of myogenic satellite cells. Cell *102*, 777-786.

Troy, A., Cadwallader, A.B., Fedorov, Y., Tyner, K., Tanaka, K.K., and Olwin, B.B. (2012). Coordination of satellite cell activation and self-renewal by Par-complex-dependent asymmetric activation of p38alpha/beta MAPK. Cell stem cell *11*, 541-553.

von Maltzahn, J., Jones, A.E., Parks, R.J., and Rudnicki, M.A. (2013). Pax7 is critical for the normal function of satellite cells in adult skeletal muscle. Proc Natl Acad Sci U S A *110*, 16474-16479.

Wilson, A., Laurenti, E., Oser, G., van der Wath, R.C., Blanco-Bose, W., Jaworski, M., Offner, S., Dunant, C.F., Eshkind, L., Bockamp, E., *et al.* (2008). Hematopoietic stem cells reversibly switch from dormancy to self-renewal during homeostasis and repair. Cell *135*, 1118-1129.

Wu, R., Li, H., Zhai, L., Zou, X., Meng, J., Zhong, R., Li, C., Wang, H., Zhang, Y., and Zhu, D. (2015). MicroRNA-431 accelerates muscle regeneration and ameliorates muscular dystrophy by targeting Pax7 in mice. Nat Commun *6*, 7713.

Xie, T., and Spradling, A.C. (2000). A niche maintaining germ line stem cells in the Drosophila ovary. Science *290*, 328-330.

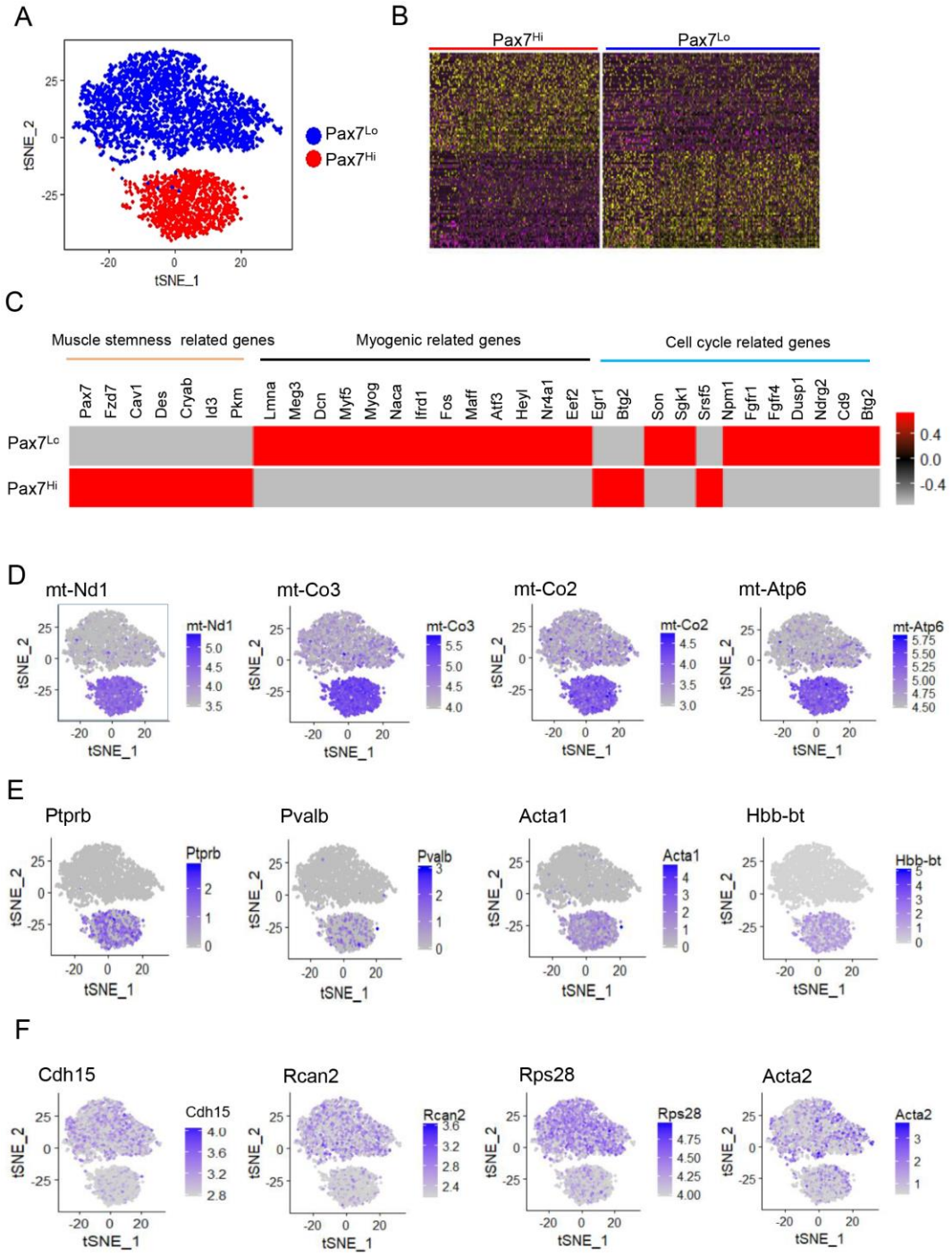

Figure 1. Transcriptional profile of Pax7^{Hi} and Pax7^{Lo} cells by single cell RNA seq

(A) 2D visualization of single-cell profiles inferred from RNA-seq data for Pax7^{Hi} and Pax7^{Lo} cells sorted from *Pax7-nGFP* mice. Each point is a single cell colored by cluster assignment.

(B) Heatmaps of normalized genes show Pax7^{Hi} and Pax7^{Lo} by top genes (columns) for individual cells (rows).

(C) Differentially expressed genes between $Pax7^{Hi}$ and $Pax7^{Lo}$ cells in heatmap view. Genes were labeled with the molecular function, as indicated.

(D) Expression patterns of *mt-Nd1*, *mt-Co3*, *mt-Co2* and *mt-Atp6* were visualized by t-SNE plots.

(E) Top unique expressed genes in $Pax7^{Hi}$ cells were visualized by t-SNE plots.

(F) Top unique expressed genes in $Pax7^{Lo}$ cells were visualized by t-SNE plots.

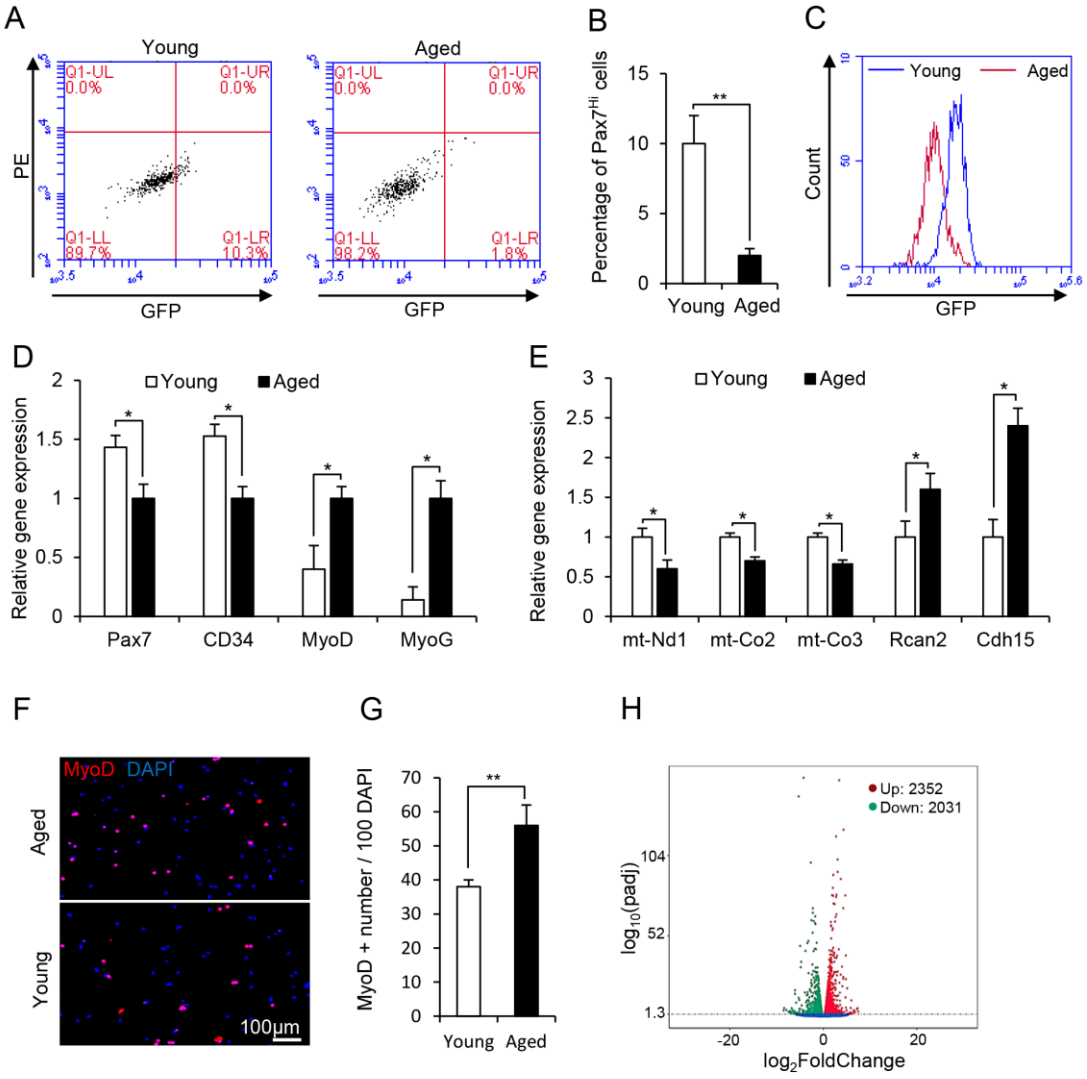

I Genes with high expression in aged muscle

GO term (BP)	Count	P-Value
cell differentiation	61	0.002753
apoptotic process	39	0.089742
lipid metabolic process	36	0.021162
response to hypoxia	19	0.014272
acyl-CoA metabolic process	7	0.00526

J Genes with high expression in young muscle

GO term (BP)	Count	P-Value
glucose homeostasis	18	0.078
cellular response to hypoxia	17	0.0185
lipid catabolic process	17	0.0299
glucose metabolic process	12	0.0353
response to glucose	12	0.0809

Figure 2. Reduced Pax7^{Hi} cells in aged mice

(A) Representative FACS profiles of Pax7 SCs from the TA muscles of aged (18-month-old) and young (3-month-old) *Pax7-nGFP* mice.

(B) The percentages of Pax7^{Hi} SCs in A were calculated. *n* = 3 for each group.

(C) Representative overall profiles of the Pax7 SCs described in A.

(D) Relative expressions of molecular markers for stemness and differentiation in FACS-resolved Pax7 SCs from the TA muscles of aged and young *Pax7-nGFP* mice, as determined by qRT-PCR. *n* = 5.

(E) Relative expressions of molecular markers for $Pax7^{Hi}$ cells and $Pax7^{Lo}$ cells in FACS-resolved Pax7 SCs from the TA muscles of aged and young *Pax7-nGFP* mice, as determined by qRT-PCR. *n* = 5.

(F) Representative images of MyoD immunostaining (red) for FACS-resolved Pax7 SCs cultured in growth medium (GM) for 18 hr. DAPI was used to visualize nuclei (blue). Scale bar represents 100 μm.

(G) The percentages of MyoD-positive cells in F were calculated from three independent experiments.

(H) Volcano plot displayed the differentially expressed genes between aged and young TA muscles. Each point represents the $\log_2$FoldChange and $\log_{10}$(padj) from three independent biological replicates. Red is upregulated genes in aged muscle compared to young one. Green is downregulated genes in aged muscle compared to young one. Blue represents genes with no change between aged and young muscle.

(I, J) Gene ontology (GO) analyses of the differentially expressed genes between aged and young TA muscle were shown as biological process (BP). The enriched GO terms for genes with high expression in aged or young TA muscle were shown in I and J, respectively. “Count” stand for the number of genes enriched in the indicated GO term. The differentially expressed genes between aged and young TA muscle were identified with cutoff (fold change > 1.5, padj < 0.05). *p< 0.05. **p< 0.01. Student’s *t*-test.

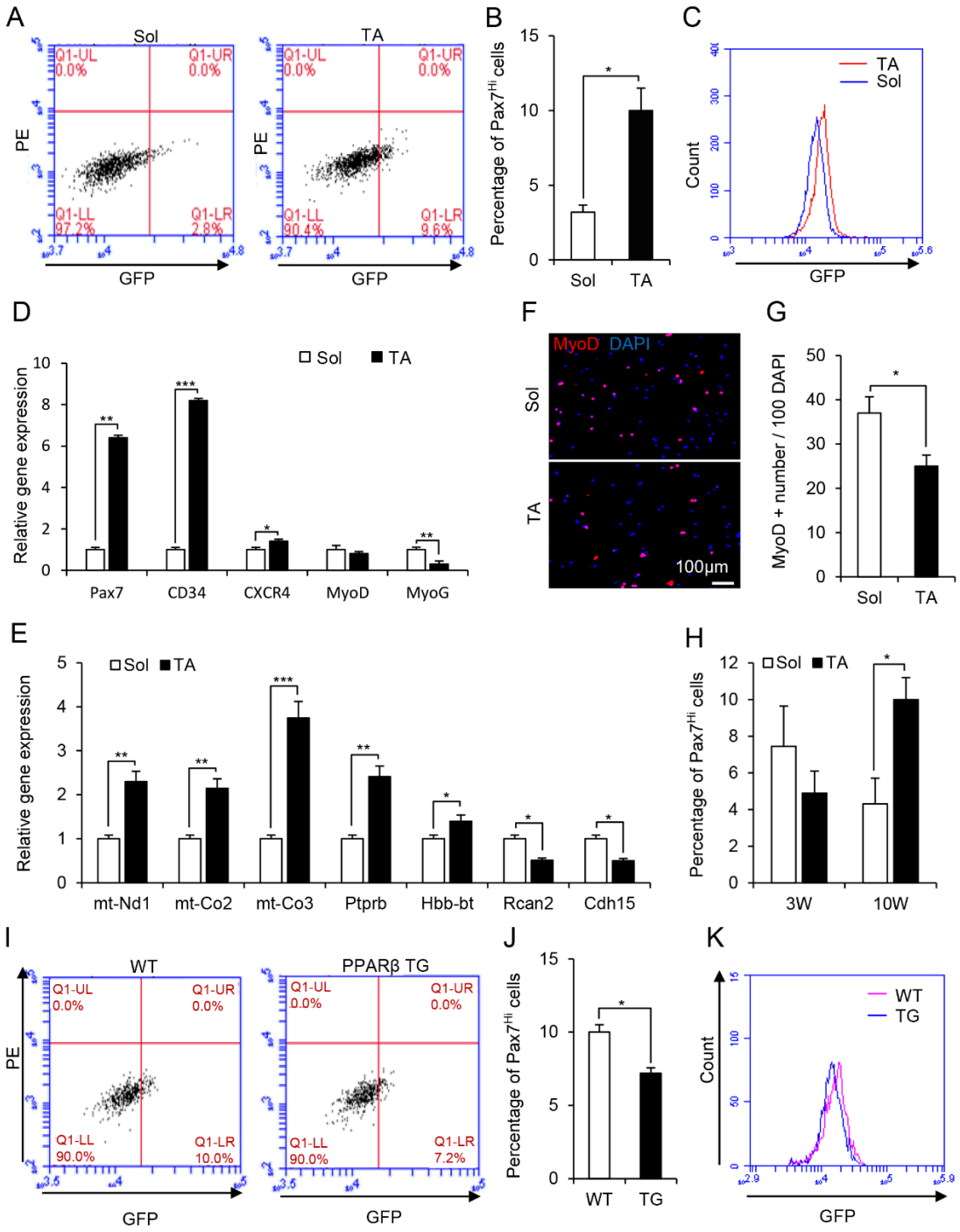

Figure 3. Glycolytic metabolism of myofiber associates with Pax7^{Hi} SC subpopulation

(A) Representative FACS profiles of Pax7 SCs sorted from the soleus (Sol) or tibialis anterior (TA) muscles of *Pax7-nGFP* mice. GFP, green fluorescence protein (488 channel); PE, phycoerythrin (594 channel).

(B) Average percentages of Pax7^{Hi} SC subpopulations obtained from three independent FACS experiments, performed as described in panel A.

(C) Representative FACS profiles of total Pax7 SCs sorted from the soleus (Sol) or tibialis anterior (TA) muscles of *Pax7-nGFP* mice. GFP, green fluorescence protein (488 channel).

(D) Relative expressions of molecular markers for stemness and differentiation in FACS-resolved Pax7 SCs from the TA and Sol muscles of *Pax7-nGFP* mice, as determined by qRT-PCR. *n* = 5.

(E) Relative expressions of molecular markers for $Pax7^{Hi}$ cells and $Pax7^{Lo}$ cells in FACS-resolved Pax7 SCs from the TA and Sol muscles of *Pax7-nGFP* mice, as determined by qRT-PCR. *n* = 5.

(F) Representative images of MyoD immunostaining (red) for FACS-resolved Pax7 SCs cultured in growth medium (GM) for 18 hr. DAPI was used to visualize nuclei (blue). Scale bar represents 100 μm.

(G) The percentages of MyoD-positive cells in F were calculated from three independent experiments.

(H) Average percentages of $Pax7^{Hi}$ SC subpopulations in TA and Sol muscle from 3 weeks and 10 weeks *Pax7-nGFP* mice. Data were obtained from three independent FACS experiments.

(I) Representative FACS profiles of total Pax7 SCs sorted from the tibialis anterior (TA) muscles of *Pax7-nGFP;MCK-PPARβ* transgenic (TG) and *Pax7-nGFP* wild-type (WT) littermates. GFP, green fluorescence protein (488 channel).

(J) The percentages of $Pax7^{Hi}$ SCs in I were calculated from three independent experiments.

(K) Representative FACS profiles of total Pax7 SCs sorted from the tibialis anterior (TA) muscles of *Pax7-nGFP;MCK-PPARβ* transgenic (TG) and *Pax7-nGFP* wild-type (WT) littermates. GFP, green fluorescence protein (488 channel). *p< 0.05. **p< 0.01. ***p< 0.001. Student's *t*-test.

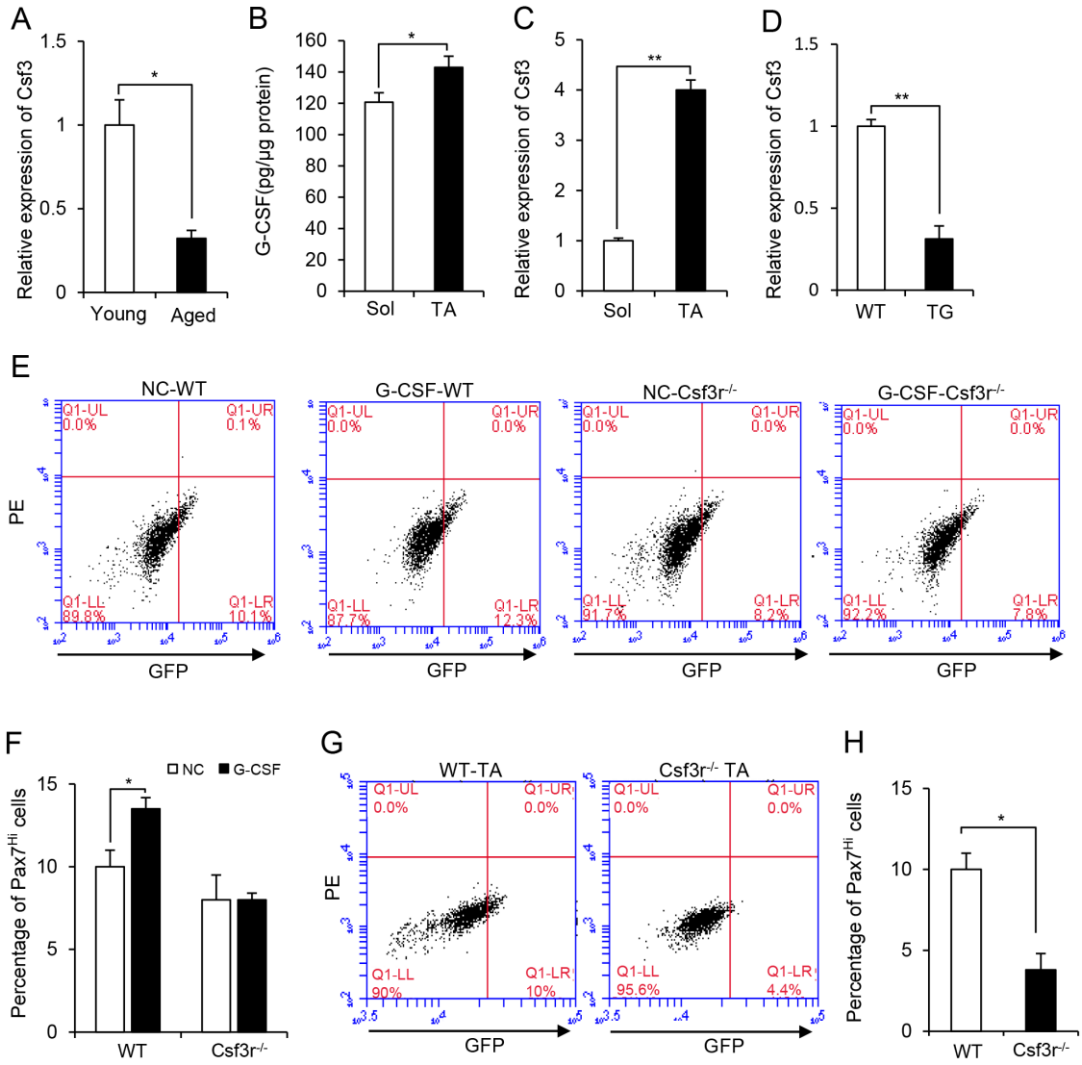

Figure 4. Muscle-released G-CSF is a Pax7 SC niche factor required for Pax7^{Hi} SCs

(A) Relative expression of *Csf3* gene in TA muscles from young (3-month-old) and aged (18-month-old) C57BL/6 mice, as determined by qRT-PCR. n = 5.

(B) G-CSF protein concentrations in TA and Sol muscles were measured with a Milliplex kit. *n* = 5.

(C) Relative expression of *Csf3* gene in single fibers isolated from TA and Sol muscles were determined by qRT-PCR. *n* = 5.

(D) Relative expression of *Csf3* gene in TA muscles from *Pax7-nGFP;MCK-PPARβ-TG* and *Pax7-nGFP* WT mice, as determined by qRT-PCR. n = 5.

(E) Representative FACS profile of Pax7^{Hi} cells in sorted Pax7 SCs treated with G-CSF in GM for 48 hr. Pax7 SCs were sorted from *Pax7-nGFP* WT and *Pax7-nGFP;Csf3r*$^{-/-}$. PBS treatment served as a negative control (NC).

(F) Average percentages of $Pax7^{Hi}$ SC subpopulations obtained from three independent FACS experiments, performed as described in panel E.

(G) Representative FACS profiles of Pax7 SCs from the TA muscles of 10-week-old *Pax7-nGFP;Csf3r*$^{-/-}$ or *Pax7-nGFP* WT mice.

(H) The percentages of $Pax7^{Hi}$ SCs in G were calculated. *n* = 3 for each genotype. *p< 0.05. **p< 0.01. Student's *t*-test.

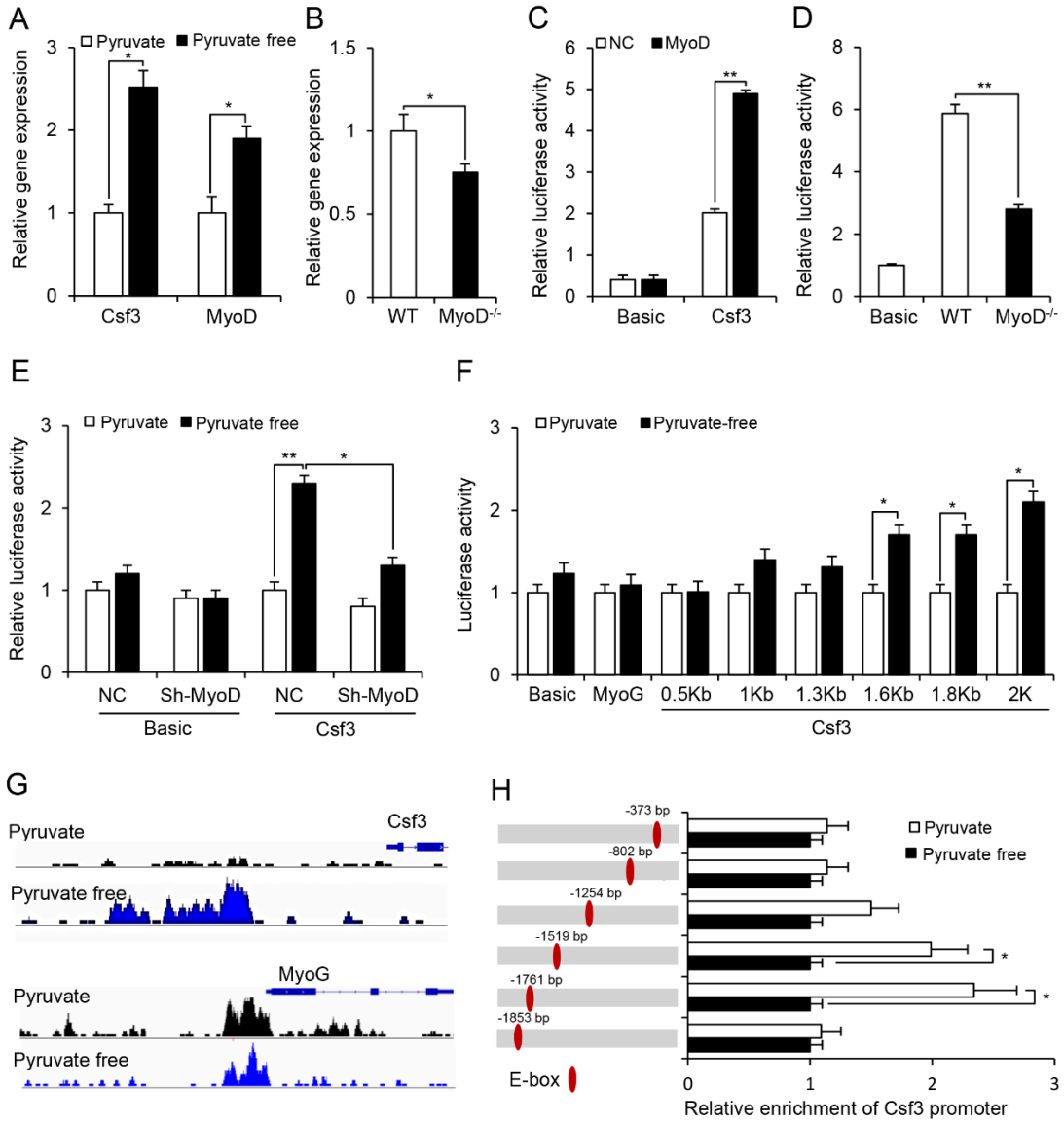

Figure 5. Expression of *Csf3* gene is metabolically regulated by MyoD in muscle cells

(A) Relative expression of *Csf3* and *MyoD* genes in C2C12 myotubes cultured in basal or pyruvate-free medium, as determined by qRT-PCR.

(B) Relative expression of *Csf3* gene in TA muscles from *MyoD*$^{-/-}$ mice and WT littermates were determined by qRT-PCR. *n* = 5 for each genotype.

(C) Relative *Csf3* promoter activities in C2C12 myotubes overexpressing MyoD were measured by dual luciferase assay. Empty vector served as a negative control (NC).

(D) Relative *Csf3* promoter activities in the TA muscles of *MyoD*$^{-/-}$ and WT littermates were measured by dual luciferase assay. *n* = 3 for each genotype.

(E) Relative *Csf3* promoter activities in MyoD-knockdown C2C12 myotubes cultured in basal or pyruvate-free medium.

(F) Relative activities of truncated *Csf3* promoter in C2C12 myotubes cultured in basal or pyruvate-free medium.

(G) ChIP-seq profiles of the *Csf3* and *MyoG* gene loci. Top to bottom: MyoD ChIP-seq profile in myotube cultured in presence of pyruvate (black signals) and absence of pyruvate (blue signals) on the promoter of *Csf3* (top panel) and *MyoG* (bottom panel).

(H) ChIP assays were performed using chromatin from myotube cultured in presence or absence of pyruvate. Chromatin was immunoprecipitated using antibodies against MyoD. The immunoprecipitated DNA was amplified using primers for *Csf3* gene promoter. *p< 0.05. **p< 0.01. Student's t-test.

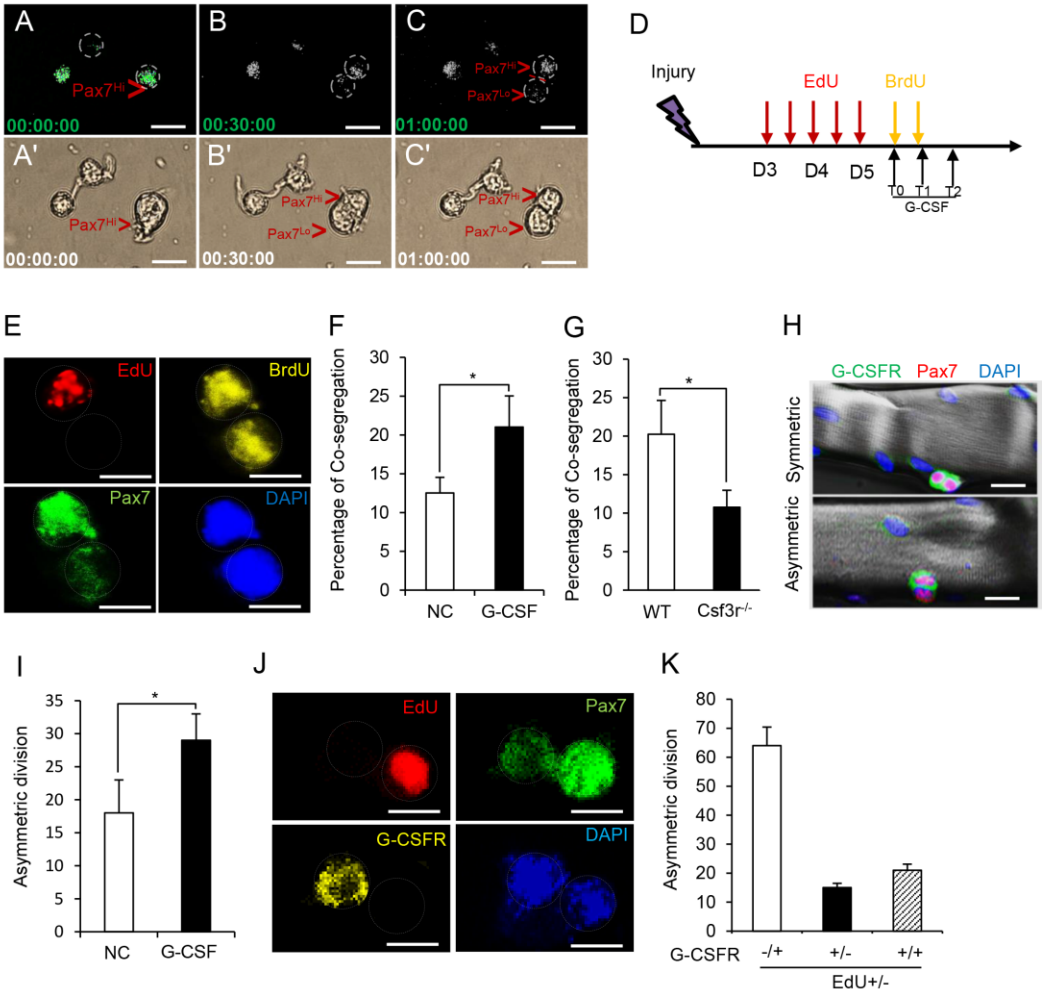

Figure 6. Muscle-derived G-CSF mediates the maintenance of the Pax7^{Hi} SC subpopulation by promoting the asymmetric division of Pax7 SCs

(A-C) Time-lapse imaging was used to trace the division of Pax7 SCs sorted from Pax7-nGFP mice. A-C were filmed in GFP channels and A'-C' were filmed in bright channels.

(D) The timing of EdU and BrdU injections (8 hr apart) used to define TDSS.

(E) Representative views showing the co-segregation of template DNA strands during the cell division of FACS-resolved Pax7 SCs from *Pax7-nGFP* mice pulse-labeled with EdU and BrdU, as characterized by EdU and BrdU staining. When old template DNA strands co-segregate, one daughter cell (EdU+/BrdU+) is a Pax7^{Hi} SC and the other (EdU-/BrdU+) is a Pax7^{Lo} SC. DAPI (blue) was used to visualize nuclei. Scale bar represents 25 μm.

(F) The percentages of EdU+/BrdU+ and EdU-/BrdU+ daughter cells observed during the cell divisions of Pax7 SCs treated with G-CSF for 24 hr. PBS treatment served as a negative control (NC). The Pax7 SCs were FACS-resolved from *Pax7-nGFP* mice pulse-labeled with EdU and BrdU.

(G) The percentages of random- and co-segregated template DNA strands observed during the cell division of Pax7 SCs from *Pax7-nGFP* and *Pax7-nGFP;Csf3r*$^{-/-}$ mice.

(H) Representative views showing the separation of G-CSFR signals (green) during the cell division of Pax7 SCs on *ex vivo*-cultured single muscle fibers. DAPI (blue) indicates nuclei. Scale bar represents 50 μm.

(I) The percentages of Pax7 SCs that show asymmetric separation of G-CSFR during cell division on *ex vivo*-cultured single fibers treated with G-CSF were calculated from three independent experiments. PBS treatments served as a negative control (NC).

(J) Representative views of the asymmetric division of G-CSFR (yellow) and co-segregation of template DNA strands (EdU-) during the cell division of FACS-resolved Pax7 SCs from *Pax7-nGFP* mice that had been pulse-labeled with EdU and cultured in GM for 24 hr. DAPI (blue) indicates nuclei.

(K) Correlation between the asymmetric division of G-CSFR in daughter cells and the co-segregation of EdU-labeled template DNA during cell division. EdU+/- GCSFR-/+ represents a doublet in which one daughter is G-CSFR-negative and EdU positive (Pax7^{Hi}) while the other is G-CSFR-positive and EdU negative (Pax7^{Lo}). *$p < 0.05$. **$p< 0.01$. Student's *t*-test.

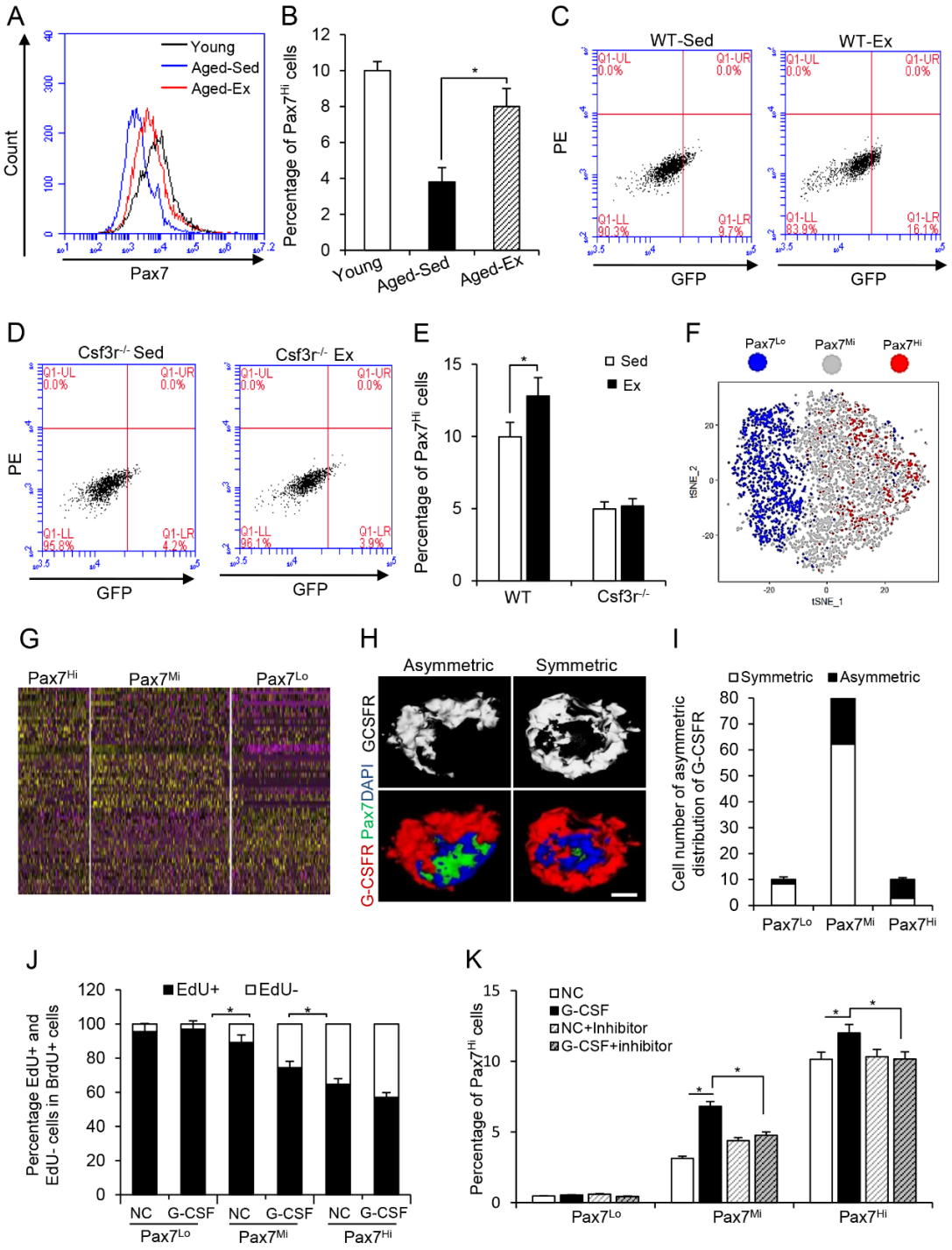

Figure 7 G-CSF replenishes Pax7^{Hi} cells by stimulating asymmetric division of Pax7^{Mi} cells

(A) Representative FACS profile of Pax7 SCs sorted by anti-Pax7 (FITC) immunostaining from the TA muscles of young, aged exercised (aged-ex), and aged sedentary (aged-Sed) C57BL/6 mice.

(B) The percentages of Pax7^{Hi} SCs in A were calculated. *n* = 3 for each group.

(C-D) Representative FACS profiles of Pax7 SCs from the TA muscles of *Pax7-nGFP;Csf3r*$^{-/-}$ or *Pax7-nGFP* WT mice subjected to exercise (Ex). Sedentary (Sed) mice served as a control. *n* = 5.

(E) The percentages of Pax7^{Hi} SCs in C and D were calculated. *n* = 3.

(F) Unsupervised clustering of Pax7^{Hi}, Pax7^{Mi} and Pax7^{Lo} cells visualized with tSNE. Each point is a single cell colored by cluster assignment.

(G) Heatmaps of normalized signal show Pax7^{Hi}, Pax7^{Mi}, Pax7^{Lo} by top genes (columns) for individual cells (rows).

(H) Representative views of the asymmetric and symmetric distributions of G-CSFR (red) in FACS-resolved Pax7 SCs obtained from *Pax7-nGFP* mice and cultured in GM for 24 hr. DAPI (blue) indicates nuclei. Scale bar represents 5 μm.

(I) The percentages of Pax7 SCs with asymmetric distribution of G-CSFR among FACS-resolved Pax7^{Hi}, Pax7^{Mi}, and Pax7^{Lo} SCs cultured in GM for 24 hr.

(J) The percentages of EdU+/BrdU+ and EdU-/BrdU+ daughter cells observed during the cell divisions of Pax7^{Hi}, Pax7^{Mi}, and Pax7^{Lo} SCs treated with G-CSF for 24 hr. PBS treatment served as a negative control (NC). The three subpopulations of Pax7 SCs were FACS-resolved from *Pax7-nGFP* mice pulse-labeled with EdU and BrdU.

(K) The percentages of Pax7^{Hi} SCs after the three subpopulations of Pax7 SCs were treated with G-CSF for 24 hr in the presence or absence of a Stat3 inhibitor, as calculated from three independent experiments. Values are presented as the mean ± s.e.m. of triplicate experiments. *p< 0.05. **p< 0.01. Student's *t*-test.

Supplemental Information

Loss of muscle stem cells in aged mice is replenished by muscle-secreted niche factor G-CSF

Hu Li[#], Qian Chen[#], Changyin Li, Ran Zhong, Yixia Zhao, Dahai Zhu*, and Yong Zhang*

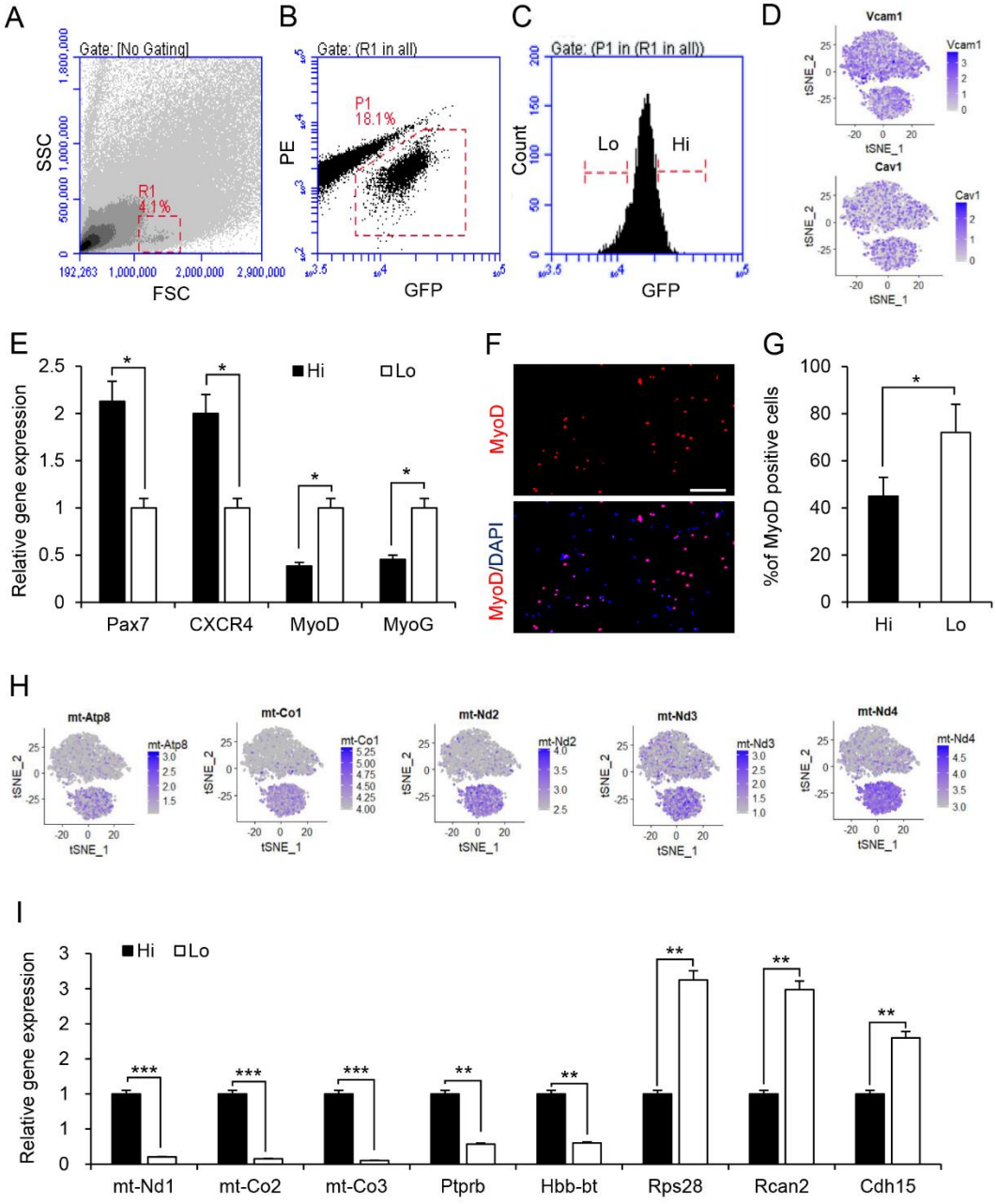

Figure S1 Characterization of FACS-sorted Pax7^{Hi} and Pax7^{Lo} cells.

(A-C) Strategy used for FACS sorting GFP+ cells from *Pax7-nGFP* mice. Gating for Pax7-nGFP^{Hi} (Pax7^{Hi}) and Pax7-nGFP^{Lo} (Pax7^{Lo}) is indicated within the total nGFP population, as previously described (Rocheteau et al., 2012). GFP, green fluorescence protein (488 channel); PE, phycoerythrin (594 channel).

(D) Expression patterns of quiescent marker of satellite cells were visualized by t-SNE plots

(E) Relative expressions of molecular markers for stemness and differentiation in FACS-resolved Pax7^{Hi} and Pax7^{Lo} SCs from the TA muscles of *Pax7-nGFP* mice, as determined by qRT-PCR. n = 5.

(F) Representative images of MyoD immunostaining (red) for FACS-resolved Pax7 SCs cultured in growth

medium (GM) for 18 hr. DAPI was used to visualize nuclei (blue). Scale bar represents 100 μm.

(G) The percentages of MyoD-positive cells in F were calculated from three independent experiments. *p< 0.05. Student's *t*-test.

(H) Expression patterns of mitochondrial genes in $Pax7^{Hi}$ and $Pax7^{Lo}$ cells were visualized by t-SNE plots.

(I) Relative expressions of molecular markers for $Pax7^{Hi}$ cells and $Pax7^{Lo}$ cells in FACS-resolved $Pax7^{Hi}$ and $Pax7^{Lo}$ from *Pax7-nGFP* mice, as determined by qRT-PCR. $n = 5$. *p < 0.05. **p< 0.01. Student's *t*-test.

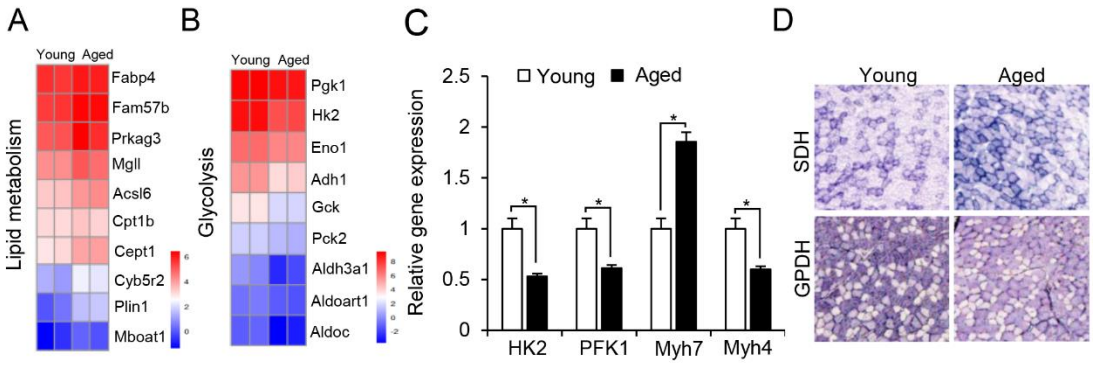

Figure S2 Muscle metabolism shift from glycolytic to oxidative during ageing

(A-B) Heatmaps indicating absolute gene expression (Log2[FPKM]) of specific metabolic regulators in aged and young muscle. Each gene listed had a mean fold change of greater than 1.5.

(C) Relative expressions of *PFK1*, *HK2, Myh7* and *Myh4* in TA muscles from young (3-month-old) and aged (18-month-old) C57BL/6 mice, as determined by qRT-PCR. $n = 5$.

(D) Representative histochemical staining of α-GPDH and SDH enzymatic activity in TA muscle of aged and young mice. *$p < 0.05$. **$p < 0.01$. Student's *t*-test.

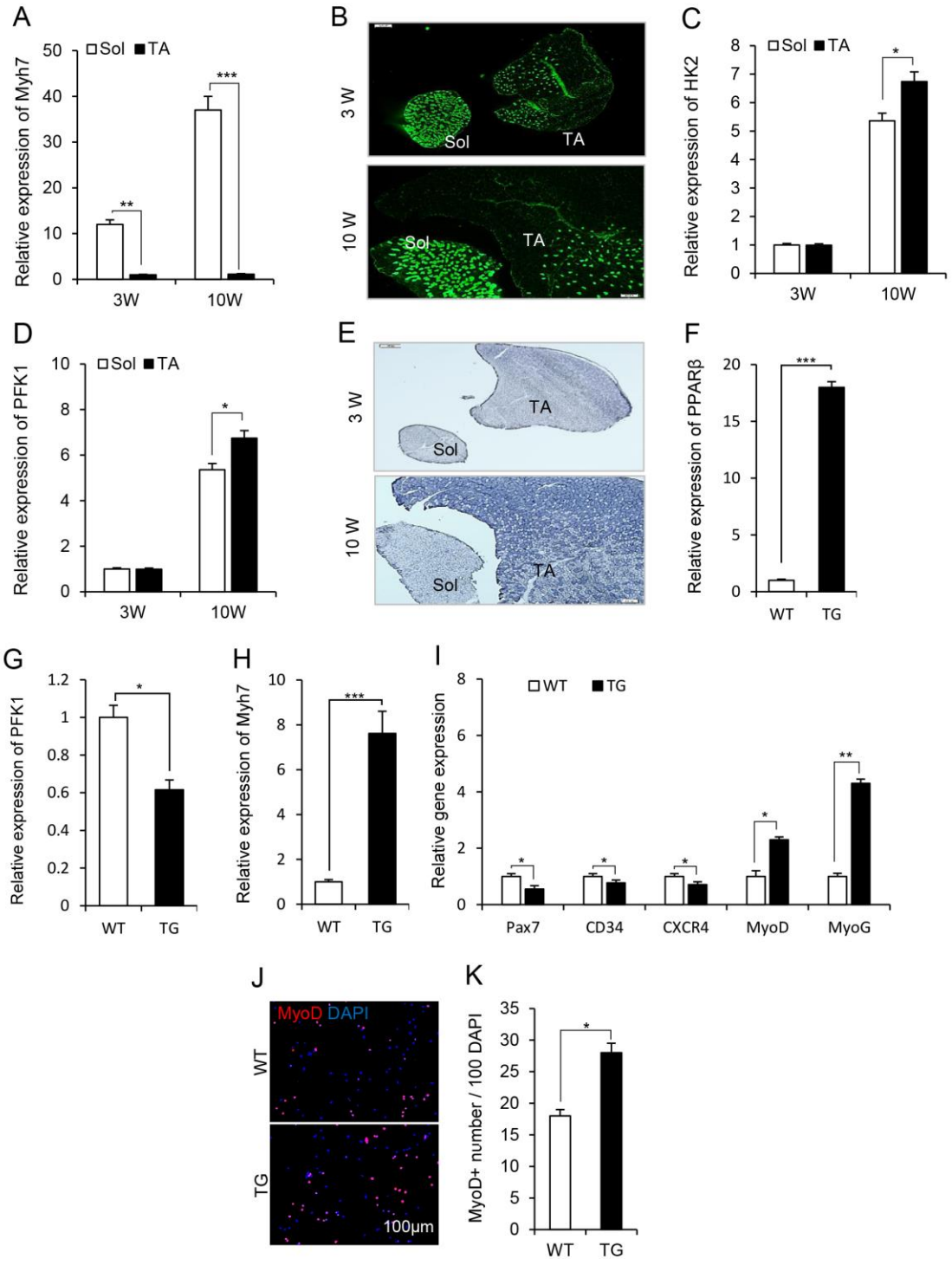

Figure S3 Fiber type composition and metabolic status in TA and Sol muscle and in TA muscle of *MCK-PPARβ-TG*.

(A) Relative expression of *Myh7* in TA and Sol muscles from 3 weeks and 10 weeks C57BL/6 mice, as determined by qRT-PCR. *n* = 5.

(B) Representative immunostaining of type I myofibers in TA and Sol muscle from 3 weeks and 10 weeks C57BL/6 mice.

(C-D) Relative expression of *HK2* (C) *and PFK1* (D) in TA and Sol muscles from 3 weeks and 10 weeks C57BL/6 mice, as determined by qRT-PCR. *n* = 5.

(E) Representative histochemical staining of α-GPDH enzymatic activity in TA and Sol muscles from 3 weeks and 10 weeks C57BL/6 mice.

(F-H) Relative expressions of *PPARβ* (F), *PFK1* (G), and *Myh7* (H) in TA muscles from *Pax7-nGFP;MCK-PPARβ*-TG (TG) and *Pax7-nGFP* WT mice, as determined by qRT-PCR. *n* = 5.

(I) Relative expressions of molecular markers for stemness and differentiation in FACS-resolved Pax7 SCs from the TA muscle of *Pax7-nGFP;MCK-PPARβ* transgenic (TG) and *Pax7-nGFP* wild-type (WT) littermates, as determined by qRT-PCR. *n* = 5.

(J) Representative images of MyoD immunostaining (red) for FACS-resolved Pax7 SCs cultured in growth medium (GM) for 18 hr. DAPI was used to visualize nuclei (blue). Scale bar represents 100 μm.

(K) The percentages of MyoD-positive cells in J were calculated from three independent experiments.

*p < 0.05. **p< 0.01. Student's *t*-test.

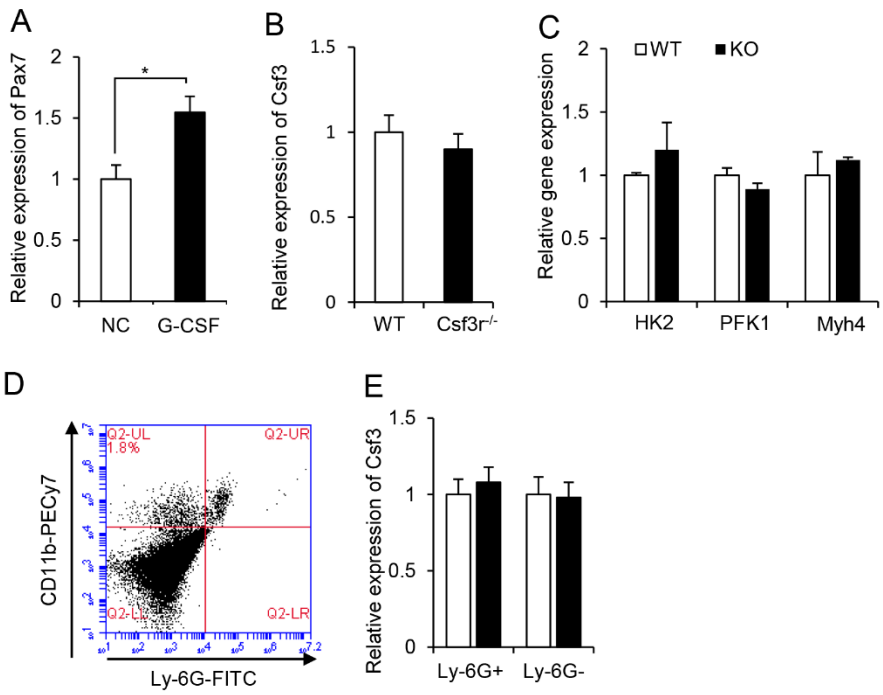

Figure S4 Muscle-released G-CSF is a Pax7 SC niche factor required for Pax7^{Hi} SCs

(A) Relative expression of *Pax7* in sorted Pax7 SCs treated with G-CSF for 48 hr, as determined by qRT-PCR.

(B) Relative expression of *Csf3* gene in TA muscle from *Pax7-nGFP;Csf3r*$^{-/-}$ mice and *Pax7-nGFP* WT littermates, as determined by qRT-PCR. *n* = 5.

(C) Relative expression of genes related to fiber type (*Myh 4*) and muscle metabolism (*HK2* and *PFK1*) in TA muscles from *Pax7-nGFP;Csf3r*$^{-/-}$ mice and *Pax7-nGFP* WT littermates, as determined by qRT-PCR. *n* = 4.

(D) Representative FACS profiles of neutrophils and macrophages. Gating for CD11b+/Ly-6G+ (neutrophils) and CD11b+/Ly-6G- (macrophages) is indicated. FITC, GFP (488 channel); PEcy7, phycoerythrin (594 channel).

(E) Relative expression of *Csf3* gene in the neutrophils and macrophages sorted in D, as determined by qRT-PCR. *n* = 4. *p < 0.05. **p< 0.01. Student's *t*-test.

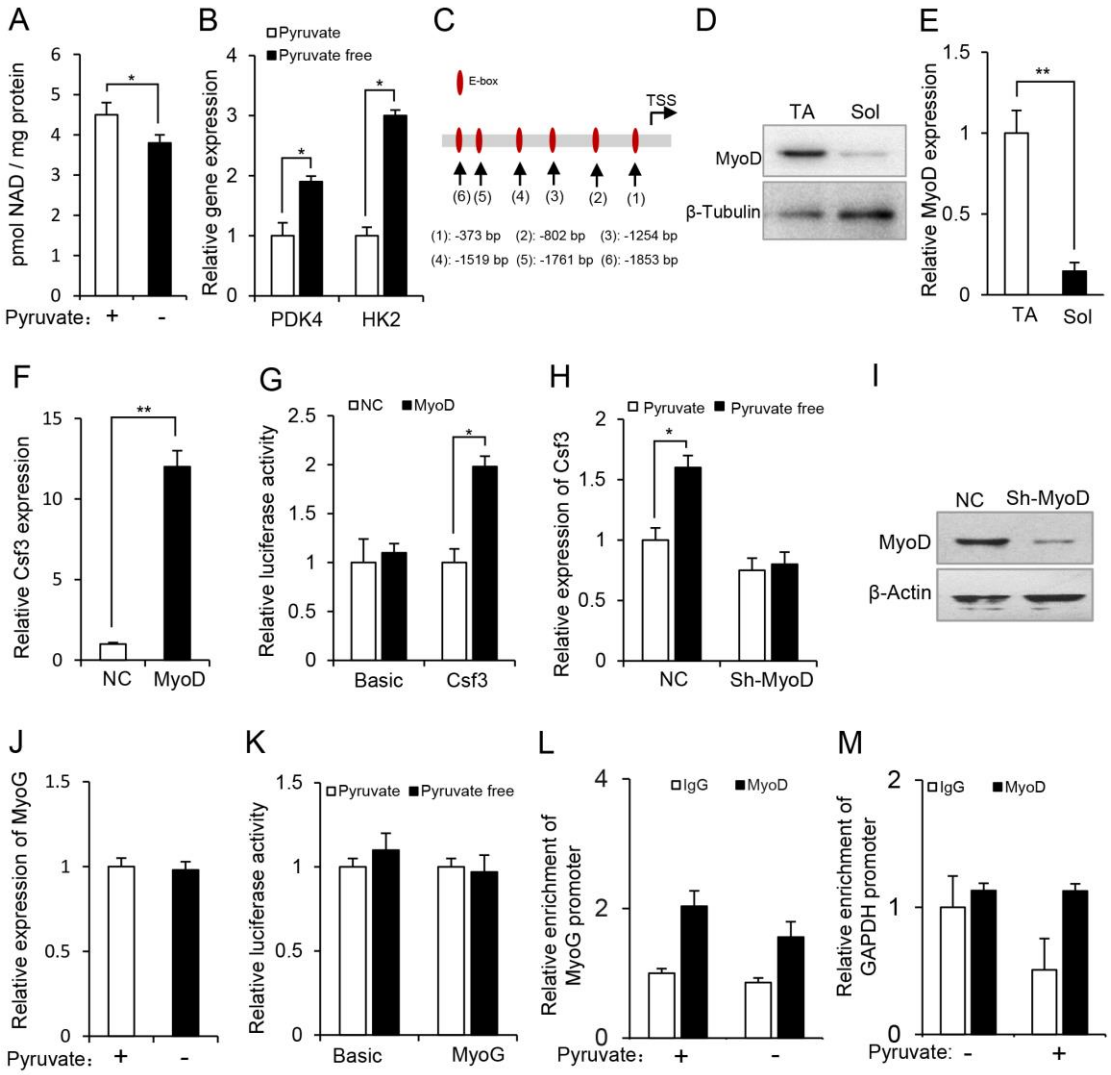

Figure S5 MyoD metabolically regulates *Csf3* gene expression in skeletal muscle cells

(A) NAD+ levels in C2C12 myotubes cultured in basal or pyruvate-free medium for 24 hr.

(B) Relative expression of *PDK4* and *HK2* in the C2C12 myotubes cultured in basal or pyruvate-free medium for 24 hr.

(C) E-boxes (CANNTG) within the 2-kb sequence upstream of the mouse *Csf3* gene.

(D) Protein levels of MyoD in TA and Sol muscles, as determined by Western blotting. β-Tubulin served as a loading control.

(E) mRNA levels of *MyoD* in TA and Sol muscles, as determined by qRT-PCR. *β-actin* served as an internal control.

(F) Relative expression of *Csf3* in C2C12 myotubes with or without (empty vector, negative control; NC) overexpression of MyoD.

(G) Relative promoter activities of the 2-kb sequence upstream of *Csf3* in fibroblasts with transient ectopic

expression of *MyoD*. Transfection with empty vector served as a negative control (NC).

(H) Relative expression of *Csf3* in MyoD-knockdown C2C12 myotubes cultured in basal or pyruvate-free medium.

(I) MyoD protein level in MyoD-knockdown C2C12 myotubes cultured in basal or pyruvate-free medium.

(J) Relative expressions of *MyoG* in C2C12 myotubes cultured in basal or pyruvate-free medium for 24 hr.

(K) Relative promoter activities of *MyoG* in C2C12 myotubes cultured in basal or pyruvate-free medium for 24 hr.

(L-M) ChIP assays were performed using chromatin from myotube cultured in presence or absence of pyruvate. Chromatin was immunoprecipitated using antibodies against MyoD. The immunoprecipitated DNA was amplified using primers for *MyoG* (L) and *GAPDH* (M) gene promoter. *p< 0.05. **p< 0.01. Student's t-test.

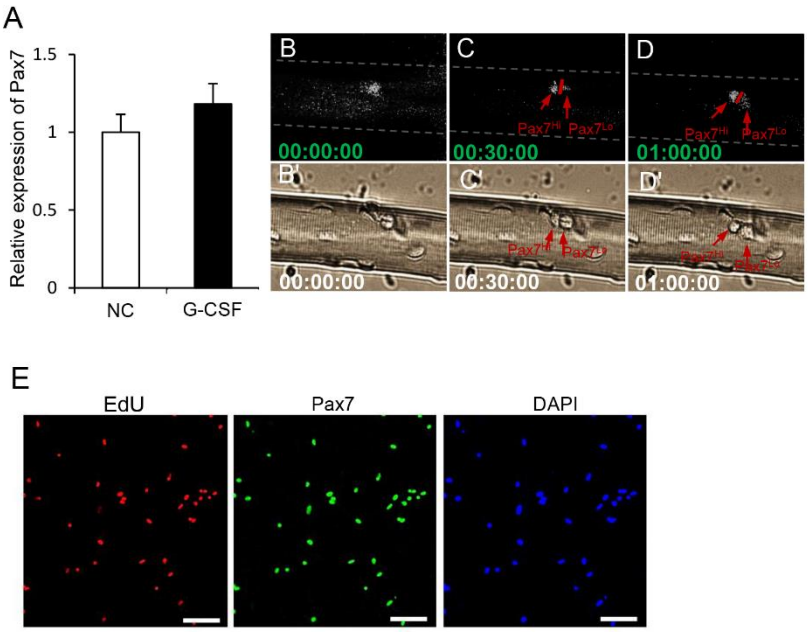

Figure S6. G-CSF promotes asymmetric division of Pax7 SCs

(A) Relative expression of *Pax7* in FACS-resolved Pax7 SCs cultured in GM containing G-CSF for 24 hr, as determined by qRT-PCR.

(B-D) Time-lapse imaging was used to trace the division of Pax7 SCs from single fibers isolated from *Pax7-nGFP* mice.

(E) Representative of EdU staining in FACS-resolved Pax7 SCs from *Pax7-nGFP* mice at T1.

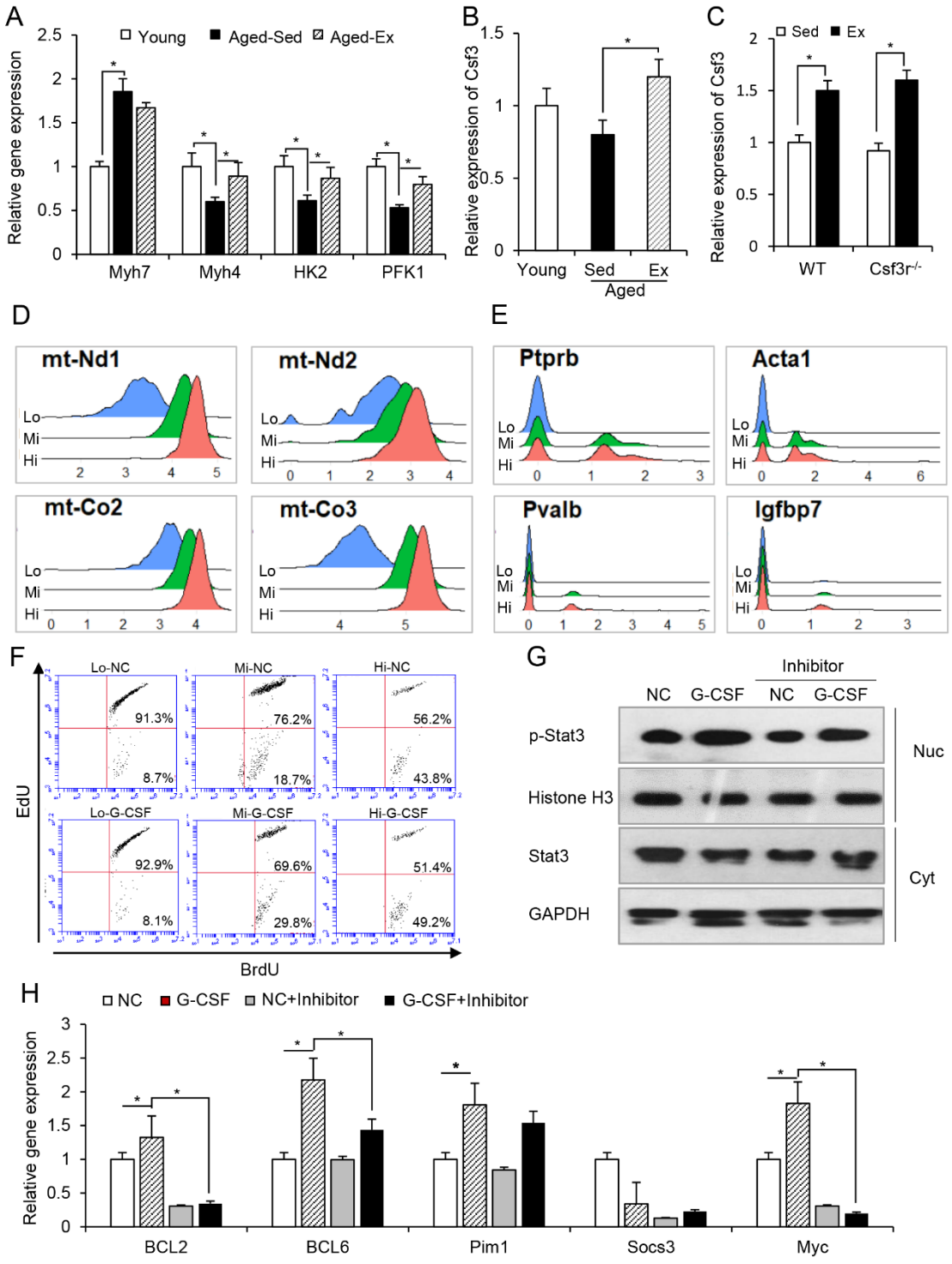

Figure S7. G-CSF replenished Pax7^{Hi} cells by promoting asymmetric division of Pax7^{Mi} cells

(A) Relative expression of *Myh7*, *Myh4*, *HK2,* and *PFK1* in TA muscles from young (Young), aged exercised (Aged-Ex), and aged sedentary (Aged-Sed) C57BL/6 mice. *n* = 5.

(B) Relative expression of *Csf3* in TA muscles from young (Young), aged exercised (Aged-Ex), and aged sedentary (Aged-Sed) C57BL/6 mice. *n* = 5.

(C) Relative expression of *Csf3* gene in the TA muscles of *Pax7-nGFP;Csf3r*$^{-/-}$ or *Pax7-nGFP* WT mice

subjected to exercise (Ex), as determined by qRT-PCR. *n* = 4.

(D) Expression patterns of mitochondrial genes of $Pax7^{Hi}$ and $Pax7^{Lo}$ cells were visualized by t-SNE plots.

(E) Representative genes in $Pax7^{Hi}$, $Pax7^{Mi}$ and $Pax7^{Lo}$ cells were visualized by Ridge plots.

(F) Flow cytometric analysis of the three subpopulations of Pax7 SCs treated with G-CSF for 24 hr and subjected to EdU and BrdU immunostaining. Numbers in corners represent percentages (%) of the cells. The three subpopulations of Pax7 SCs were sorted from Pax7-nGFP mice and pulse-labeled with EdU and BrdU.

(G) Protein levels of Stat3 and p-Stat3 in Pax7 SCs treated with G-CSF in the presence or absence of the Stat3 inhibitor, 5,15 DPP, as determined by Western blotting. GAPDH and histone H3 served as loading controls for the cytoplasmic and nuclear fractions, respectively.

(H) Relative expressions of *BCL2*, *BCL6*, *Pim1*, *Socs3*, and *Myc* in Pax7 SCs treated with G-CSF in the presence or absence of 5,15 DPP, as determined by qRT-PCR. Values are presented as the mean ± s.e.m. of data from three independent experiments. *p< 0.05. Student's t-test.

Materials and Methods

Mouse lines and animal care

Pax7-nGFP Tg mice were kindly gifted by Dr. Shahragim Tajbakhsh (Institute Pasteur, France). *MCK-PPARβ* transgenic (TG) mice were kindly gifted by Dr. Zhenji Gan (Nanjing University, China). *Csf3r*$^{-/-}$(#017838) and *MyoD*$^{-/-}$ (#002523) mice were obtained from the Jackson Laboratory. Mice were housed in an animal facility and given free access to water and standard rodent chow. All animal procedures were approved by the Animal Ethics Committee of Peking Union Medical College, Beijing (China).

Fluorescence activated cell sorting (FACS)

Pax7 SCs from the skeletal muscles of *Pax7-nGFP*, *Pax7-nGFP;MCK-PPARβ* TG, and *Pax7-nGFP;Csf3r*$^{-/-}$mice were fluorescently sorted as previously described (Wu et al., 2015). Briefly, mononuclear muscle-derived cells were isolated from the tibialis anterior (TA) and soleus (Sol) muscles of *Pax7-nGFP* reporter mice (8-week-old males) by dispase and collagenase digestion, filtered through 70-μm and 40-μm cell strainers, and directly sorted with a BD Aria II Cell Sorting System. Pax7 SCs from the skeletal muscles of C57BL/6 non-reporter mice were fluorescently sorted as previously described (Wu et al., 2015). These mononuclear cells from the skeletal muscles of C57BL/6 mice were blocked with goat serum for 10 min and incubated with FITC-CD45 (BD, 553080), FITC-CD31 (BD, 553372), PE-Sca1 (BD, 553108), biotin-VCAM (BD, 553331), and streptavidin-APC (BD, 554067) antibodies in Dulbecco's modified Eagle's medium (DMEM) with 2% fetal bovine serum (FBS) for 15 min at 4°C. Immunostained cells were briefly washed and passed through a 40-μm nylon mesh (Falcon). SCs ($CD45^{-}CD31^{-}Sca1^{-}Vcam^{+}$) were further separated with the BD Aria II and subsequently immunostained with Pax7 antibody (DSHB). The $Pax7^{Hi}$ and $Pax7^{Lo}$SC subpopulations were further analyzed with the BD Aria II. The sorting gates used for the $Pax7^{Hi}$ and $Pax7^{Lo}$SC subpopulations were as previously described(Rocheteau et al., 2012). Cells were labeled with propidium iodide (PI) 10 μg/ml (Sigma-Aldrich) to exclude dead cells and displayed using the PE (Phycoerythrin, red) channel on the FACS profile.

To sort immune cells from TA and Sol muscles, single-cell suspensions were prepared using dispase and collagenase, blocked with goat serum for 10 min, and co-incubated with CD11b-

PECy7 (BD, 561098) and Ly-6G-FITC (BD, 561105) in DMEM supplemented with 2% FBS for 15 min at 4°C. The immunostained cells were briefly washed, passed through a 40-μm nylon mesh (Falcon), suspended at 10^3-10^7 cells/ml, and further separated with the BD Aria II. The sorting gates were strictly defined on the basis of mono-antibody-stained control cells and the forward- and side-scatter patterns obtained from the cells of interest in preliminary tests.

Single cell RNA Seq using the 10x Genomics Chromium Platform

scRNA-seq libraries were prepared with the Single Cell 30 Reagent Kit as instruction from User Guide v2 (10x Genomics). Cellular suspensions of $Pax7^{Hi}$, $Pax7^{Mi}$ and $Pax7^{Lo}$ were loaded on a Chromium Controller instrument (10x Genomics) to generate single-cell gel bead-in emulsions (GEMs), respectively. GEM-reverse transcriptions (GEM-RTs) were performed in a Veriti 96-well thermal cycler (Thermo Fisher Scientific). After RT, GEMs were harvested and the cDNAs were amplified and cleaned up with the SPRIselect Reagent Kit (Beckman Coulter). Indexed sequencing libraries were constructed using the Chromium Single-Cell 30 Library Kit (10x Genomics) for enzymatic fragmentation, end-repair, A-tailing, adaptor ligation, ligation cleanup, sample index PCR, and PCR cleanup. Sequencing libraries were loaded on a HiSeqX10 (Illumina). Reads were aligned to mm9 reference assembly. Primary assessment with this software for the $Pax7^{Hi}$ sample reported 1469 cell-barcodes with 4466 median unique molecular identifiers (UMIs, transcripts) per cell and 1496 median genes per cell sequenced to 96.7% sequencing saturation with 313,083 mean reads per cell. Primary assessment with this software for the $Pax7^{Mi}$ sample reported 5859 cell-barcodes with 3465 median unique molecular identifiers (UMIs, transcripts) per cell and 1260 median genes per cell sequenced to 94.9% sequencing saturation with 354,032 mean reads per cell. Primary assessment with this software for the $Pax7^{Lo}$ sample reported 2982 cell-barcodes with 4317 median unique molecular identifiers (UMIs, transcripts) per cell and 1478 median genes per cell sequenced to 97.1% sequencing saturation with 300,302 mean reads per cell.

Statistical method of Single cell RNA Seq

We used Cell Ranger version 1.3.1 (10x Genomics) to process raw sequencing data and Seurat suite version 2.0.0 for downstream analysis. The Seurat R package were used for graph-based clustering and visualizations, all functions mentioned are from this package or the standard R version 3.4.2 package unless otherwise noted and were used with the default

parameters unless otherwise noted. Initially, we merged the three libraries by Seurat and we analyzed only cells (unique barcodes) that passed quality control processing (above) and expressed at least 500 genes and only genes that were expressed in at least 3 cells. We also removed cells with greater than 1% mitochondrial genes. We applied library-size normalization to each cell with Normalize Data. Normalized expression for gene i in cell j was calculated by taking the natural log of the UMI counts for gene i in cell j divided by the total UMI counts in cell j multiplied by 10,000 and added to 1. To reduce the influence of variability in the number of UMIs, mitochondrial gene expression between cells on the clustering, we used the ScaleData function to linearly regress out these sources of variation before scaling and centering the data for dimensionality reduction. Principle component analysis was run using RunPCA on the variable genes calculated with FindVariableGenes (x = (0.1,6), y = (0.5, 15) and then extended to the full dataset with ProjectPCA. Based on the PCElbowPlot result we decided to use 1 and 10 principle components (PCs) for the clustering of cells. We ran FindClusters to apply shared nearest neighbor (SNN) graph-based clustering to each sample (0.6).

RNA seq

Total RNA were isolated from TA muscle of young (2-month-old) and aged (18-month-old) mice with Trizol reagent (Invitrogen). Sequencing libraries were generated using NEBNext super speed RNA Library Prep Kit for Illumina following the manufacturer's recommendations. Raw-sequencing data were mapped to the mouse genome mm9 assembly using the TopHat44 with default parameters. DEGSeq45 was used to calculate the read coverage for each gene. Related data were submitted to GEO with the accession number GSE. Differentially expressed genes were filtered using a change greater than twofold and p-value (0.05) as a criterion for differential expression. Differentially expressed genes were validated using the iQ5 Multicolor Real-Time PCR Detection System (Bio-Rad). The primer sequences were designed using DNAMAN. Pax7-(s) CCGTGTTTCTCATGGTTGTG，(as) GAGCACTCGGCTAATCGAAC; MyoD-(s) CAACGCCATCCGCTACAT, (as) GGTCTGGGTTCCCTGTTCT; MyoG-(s)-CCATTCACATAAGGCTAACAC, (as)-CCCTTCCCTGCCTGTTCC; Csf3-(s)-AGTGCACT ATGGTCAGGACGAG，(as) GGATCTTCCTCACTTGCTCCA; Nd1-(s) CATACCCCCGA TTCCGCTAC, (as) GTTTGAGGGGGAATGCTGGA; Co3-(s) ACCAATGATGGCGCGA TGTA, (as) GGCTGGAGTGGTAAAAGGCT; Co2-(s) CCGTCTGAACTATCCTGCCC, (as)

GAGGGATCGTTGACCTCGTC; Ptprb-(s) GCTGCCACGGCCCTT; (as) CTCTGCCACTC CAGTCTGC; Pvalb-(s) ACACTGCAGCGCTGGTCATA, (as) AGGAGTCTGCAGCAGCA AAGG; Rps28-(s) GGTGACGTGCTCACCCTATT, (as) CCAGAACCCAGCTGCAAGAT

Chromatin Immunoprecipitation (ChIP)

ChIP analyses were performed on chromatin extracts from myotube cultured with or without pyruvate according to the manufacturer's standard protocol (Millipore, Cat. #17-610) using antibodies against MyoD (Santa Cruz, SC-760). Briefly, cells were lysed in RIPA buffer (PBS, 1% NP-40, 0.5% sodium deoxycholate, 0.1% SDS) and centrifuged at 800 × g for 5 min. The chromatin fraction was sheared by sonication in 1.5 ml siliconized Eppendorf tubes. The resulting sheared chromatin samples were cleared for 1 hr, immunoprecipitated overnight, and washed in buffer I (20 mM TrisHCl [pH 8.0], 150 mM NaCl, 2 mM EDTA, 0.1% SDS, 1% Triton X-100), buffer II (20 mM TrisHCl [pH 8.0], 500 mM NaCl, 2 mM EDTA, 0.1% SDS, 1% Triton X-100), buffer III (10 mM Tris HCl [pH 8.0], 250 mM LiCl, 1% NP- 40; 1% sodium deoxycholate, 1 mM EDTA), and Tris-EDTA (pH 8.0). All washes were performed at 4℃ for 5 min. Finally, crosslinking was reversed in elution buffer (100 mM sodium bicarbonate [NaHCO3], 1% SDS) at 65℃ overnight. The resulting DNA were subjected to library construction for sequencing.

Analysis of ChIP sequencing (ChIP-Seq)

ChIP-Seq data were obtained using an Illumina HiSeq 2000, with samples de-multiplexed via the Illumina pipeline, and mapped to the mouse genome (UCSC genome browser, mm9 version) using the Bowtie algorithm. ChIP-Seq data generated from mock DNA immunoprecipitates (input DNA) were used against the sample data in calling enriched regions and to control for the false-positive detection rate (FDR). MyoD peaks were called using MACS version 1.4.1, with p-value set to 10^{-5} for enrichment against the input genomic DNA, background reads were shuffled and randomly down sampled to adjust for the difference in read coverage between samples. Downstream analyses to generate intensity profile around the transcriptional start site (TSS), and correlative analysis with RNA-Seq data were completed using custom written codes in MATLAB. Fold enrichment was also quantified using qRT–PCR. The primer sequences were designed using DNAMAN. Primer 1-(s) ATCACAAATGAAGGGCAGAG, (as) CAAGACTGCTTCTGTCTCTCC; Primer 2-(s) ATGAGCAGAGATCGTCGGGA, (as)

CACATTACCTCGATGTCGTG; Primer 3-(s) TGTCCTCTCAAGCAGAGGCTAT, (as) GATGTTGAGGCATACCTGATG; Primer 4-(s) CGCAAGATGTCTATCTG, (as) CCATGCCCGGCGAGATTTAATTC; Primer 5-(s) CTTGTGCAGCTCATCAAGGC, (as) GTGGTGGGGATCTTTTGCTG; Primer 6-(s) GCTACATTCTGAACGCTGCC, (as) GCCTTGATGAGCTGCACAAG.

SDH and GPDH staining

For measurement of succinate dehydrogenase (SDH) activity, muscles were harvested and serial tissue cross-sections (10-µm) were cut at -20°C and adhered to glass coverslips. The coverslips were inverted and placed over a microscope slide reaction chamber. The tissue was first incubated in the dark at 23°C in a substrate-free blank solution consisting of 1 mM sodium azide, 1 mM l-methoxyphenazine methosulfate (MPMS), 1.5 mM NBT, and 5 mM EDTA in 100 mM sodium phosphate buffer (pH 7.6). The reaction was allowed to proceed for 10 min to allow the nonspecific staining to plateau. The blank was then replaced with a substrate solution consisting of the above reagents plus 48 mM succinic acid. Images were captured every 3times for 10 min. For measurement of α-glycerophosphate dehydrogenase (α-GPDH) activity, serial sections (14-µm) were cut, adhered to glass coverslips, and distributed between two Coplin jars kept at -20°C. A blank solution consisting of 1 mM sodium azide, 1 mM MPMS, and 1.2 mM NBT in 100 mM sodium phosphate buffer (pH 7.4, 37ºC) was added to one jar while a solution of the above reagents plus 9.3 mM α-glycerophosphate was introduced into the other for the substrate reaction. The tissue sections were incubated in the dark for 24 min at 37°C, the reactions were stopped by extensive rinsing with distilled water. The images were captured using a microscope (Olympus).

Luminex-based identification of muscle-secreted cytokines

A mouse growth factor magnetic bead 96-well plate assay kit (MAGPMAG-24K, Millipore), which utilizes LuminexxMAP technology, was used to identify muscle-secreted factors according to the provider's instructions. Briefly, tibialis anterior (TA) and soleus (Sol) muscles from C57BL/6 mice were homogenized in PBS buffer containing a protease inhibitor cocktail. Each muscle homogenate (25 µl, 3 µg/ml) was incubated with color-coded bead sets specific to each cytokine. A biotinylated detection antibody was introduced, and the sample was incubated with streptavidin-phycoerythrin, which acted as the reporter molecule on the surface

of each microsphere. After immunoreaction, the plate was run on a Bio-plex 200^{TM} (BioRad). Finally, the median fluorescence intensity (MFI) data were analyzed using a five-parameter logistic method to calculate the concentration of each cytokine in the examined samples.

Isolation and staining of single myofibers

Single myofibers were isolated from the EDL muscles of 8-week-old *Pax7-nGFP* mice by digestion with collagenase I (Sigma, C-0130), as previously described (Wu et al., 2015). Briefly, each muscle sample was incubated in 3 ml of 0.2% collagenase I in serum-free DMEM in a shaking water bath at 37°C for 45-60 min. Digestion was considered complete when the muscle looked less defined and slightly swollen, with hair-like single fibers flowing away from the edges. The digested muscles were placed in a Petri dish, and myofibers were isolated under a microscope. Single fibers were placed in six-well plates pre-coated with horse serum, and then given 2 ml/well of fiber medium (DMEM supplemented with 20% FBS, 0.5% chick embryo extract, 10 pg/ml G-CSF, and penicillin-streptomycin). The fibers were cultured for 48hr at 37°C in a 5% CO_2 atmosphere, fixed with 4% paraformaldehyde, and stained for G-CSFR. The fibers were then washed with PBS containing 0.1% BSA and incubated for 2 hr with fluorescein-conjugated secondary antibodies (Zhongshanjinqiao Corporation) and Hoechst or DAPI. For statistical analyses, the cells with symmetric and asymmetric distribution of G-CSFR were counted in at least 100 doublets per mouse. Five mice were assayed in each set of experiments.

Immunofluorescence

FACS-resolved Pax7 SCs were seeded on collagen-coated glass slides in 24-well plates (2×10^4 cells/cm^2) in growth medium (F-10 containing 20% FBS) for 24 hr, fixed with 4% formaldehyde for 5 min, permeabilized in 0.1% Triton-X100 in PBS for 15 min at room temperature, and then blocked with 3% bovine serum albumin for 30 min. For BrdU immunostaining, the cells were unmasked with 2 N HCl for 20 min at room temperature and neutralized with 0.1 M sodium tetraborate. The cells were incubated with primary antibodies against MyoD (Santa Cruz, SC-760), G-CSFR (Santa Cruz, SC-9173), Numb (Abcam, ab14140), EdU (Invitrogen, C10640) and BrdU (Abcam, ab6326) overnight at 4ºC. The cells were then washed with PBS containing 0.1% BSA and incubated for 2 hr with fluorescein-conjugated secondary antibodies (Zhongshanjinqiao Corporation) and Hoechst or DAPI. After

several washes with PBS, the cells were examined under a fluorescence microscope (Olympus).

Western blot analysis

TA and Sol muscles from C57BL/6 mice were homogenized in a buffer containing 50 mM Tris pH 7.5, 150 mM NaCl, 0.5% Nonidet P40, and protease and phosphatase inhibitors. The muscle homogenates were clarified by centrifugation at 12,000 × g for 10 min. Total proteins (40 μg) were resolved by SDS-PAGE, transferred to a polyvinylidene fluoride membrane, and immunoblotted with primary antibodies against MyoD (Santa Cruz, SC-760) andβ-tubulin (Santa Cruz, SC-5274) overnight at 4ºC. For Stat3 detection, the FACS-sorted Pax7 SCs were treated with G-CSF (10 pg/ml) in presence or absence of Stat3 inhibitor, 5,15 DPP (50 μM, Sigma-Aldrich), in growth medium for 48 hr. Subsequently, the nuclear and cytoplasmic fractions were further isolated from the treated SCs with the kit (Thermo, 78835). The nuclear (10 μg) and cytoplasmic protein (15 μg) were resolved by SDS-PAGE, transferred to a polyvinylidene fluoride membrane, and immunoblotted with primary antibodies against Stat3 (Abcam, ab19352), p-Stat3 (CST, 9154), histone H3 (Abcam, ab1797) and GAPDH (Millipore, Mab374).Membranes were washed for 30 min, incubated with horseradish peroxidase-conjugated secondary antibodies (Zhongshanjinqiao Corporation) for 1 hr at room temperature, and washed for 30 min. Each membrane was then placed into Detection Solution (Thermo), incubated for 1 min at room temperature, and exposed to X-ray film.

RNA extraction and qRT-PCR

Total RNA was extracted from skeletal muscles using the TRIzol reagent (Invitrogen) and reverse transcribed with reverse transcriptase (Fermentas). Real-time quantitative PCR analyses were performed in triplicate using the Fast Eva Green qPCR Master Mix (BioRad). *β-actin* was used as an internal control for qRT-PCR analyses.

Treadmill

Young (3-month-old) and aged (18-month-old) *Pax7-nGFP;Csf3r*$^{-/-}$ mice, their wild-type littermates (*Pax7-nGFP*),and aged C57BL/6 mice were subjected to treadmill exercise using an Exer3/6 (Columbus Instruments). Mice were acclimated to treadmill running four times (every other day) before the test. Each mouse ran on the treadmill at 20° downhill, starting at a speed of 10 cm/s. After 3 min, the speed was increased by 2 cm/s to a final speed of 20 cm/s. Then the mice were allowed to run 25 min. After exercise training, the mice were sampled for

purification and analysis of $Pax7^{Hi}$ and $Pax7^{Lo}$ SCs.

Cell culture and treatments

FACS-resolved Pax7 SCs were cultured in F-10 medium containing 20% FBS and 2.5 ng/ml bFGF (Invitrogen) in the presence or absence of G-CSF (10 pg/ml, Santa Cruz) at 37°C in a 5% CO_2 atmosphere. Fibroblasts (C3H-10T1/2, ATCC) were cultured in DMEM (Gibco) supplemented with 4.5 g/L glucose, 10% FBS, and 1% penicillin/streptomycin at 37°C in a 5% CO_2 atmosphere. C2C12 cells (ATCC) were cultured in growth medium consisting of DMEM supplemented with 20% FBS and 1% penicillin/streptomycin. At 70–80% confluence, the C2C12 cells were switched to differentiation medium (DMEM with 2% horse serum). After 5 days of differentiation, the C2C12 myotubes were cultured in differentiation medium with or without pyruvate for 24 hr. For MyoD overexpression or knockdown, C2C12 myotubes were transiently transfected with pEGFPN1-MyoD or LV-sh-MyoD using Lipofectamine2000 (Invitrogen). The empty vector served as the negative control (NC).

Luciferase reporter assay

To test promoter activity, a 2-kb sequence upstream of the *Csf3* gene was retrieved from the University of California Santa Cruz genome browser and cloned into the pGL3 Basic vector carrying the firefly luciferase gene (Promega). The generated pGL3-G-CSF-2k was used to transfect C3H-10T1/2 cells or C2C12 myotubes in differentiation medium with or without pyruvate. Empty pGL-3 vector was used as a negative control, and co-transfection with a Renilla luciferase plasmid (Promega) served as a transfection control. The results are expressed as the activity of firefly luciferase relative to that of Renilla luciferase. For promoter reporter gene assays *in vivo*, mouse TA muscles were injected with 20 μg of apGL3-G-CSF-2k plasmid DNA with electroporation. Briefly, plate electrodes were positioned on each side of the leg over the TA muscle, in contact with the skin. TA muscles were stimulated eight times (parameters: 100 V, duration 20 ms, interval 100 ms) with a stimulator (EM830, BTX).The same amount of empty pGL3 Basic vector served as a negative control. 5μgof Renilla luciferase plasmid were co-injected as a normalization control. Luciferase activity assays were performed with homogenates of TA muscle 24 hr after electroporation.

Time-lapse imaging

Sorted Pax7 SCs or isolated single fibers from *Pax7-nGFP* mice were plated on a 24-well

plate pre-coated with matrigel. After incubation overnight, the cells were filmed with a Real-Time Cell History Recorder (JuLi stage, NanoEnTek Inc., Korea) inside an incubator. Images were taken every 15 min using the bright and GFP channels. The raw data were transformed and are presented as a video.

Template DNA strand segregation (TDSS)

Template DNA strand segregation was analyzed as previously reported (Rocheteau et al., 2012). Briefly, the TA muscles of *Pax7-nGFP* mice (6- to 10-week-old) were injured by intramuscular injection of cardiotoxin (CTX; 50 µl of 10-µM CTX per TA muscle). Mice were injected intraperitoneally 3 days post injury with EdU (five times, 200 mg/injection, 8 hr apart) followed by injection of BrdU (twice, 8 hr apart). Then Pax7 SCs were sorted, cultured in DMEM for a further 24 hr, and immunostained with anti-BrdU (1:300, Abcam) and EdU (1:300, Invitrogen).

Measurement of NAD

NAD^+ and NADH were determined using commercially available kits (Biovision, Milpitas) according to the provider's instructions.

Statistical analysis

Values are presented as means ± s.e.m. The statistical significance of the difference between two means was calculated using the two-tail Student's *t*-test. $p<0.05$ was considered statistically significant.